Co
20 Cr
15 W
10 Ni

L-605

1 **GENERAL**

L-605 is a high temperature cobalt-base superalloy originally introduced in the early 1950s. It combines solution strengthening by tungsten with second phase strengthening by precipitated carbides. It exhibits high strength up to 1500 F and good oxidation resistance to 2000 F. The alloy is also fabricable, weldable, and machinable. L-605 is sensitive to silicon, which promotes the formation of Co_2W Laves phase during exposure at 1400 to 1700 F and subsequent reduced ductility at room temperature. Major applications for L-605 are in the hot sections of aircraft gas turbine engines and include combustor liners (wrought sheet), vanes (cast), and other parts requiring moderate strength and good oxidation resistance at high temperatures. L-605 is also used as a seal in the space shuttle main engine and has been evaluated for re-entry heat shield applications. It is available in a large range of forms including sheet, plate, bar, wire, forgings, and investment castings (59,60).

1.01 **Commercial Designation**

L-605.

1.02 **Alternate Designations**

Haynes Alloy No. 25, WF-11, Unitemp L-605, AISI 670, UNS R30605.

1.03 **Specifications**

1.031 Specifications, Table 1.031.

1.04 **Composition**

1.041 Composition, Table 1.041.

High silicon content results in reduced hot forgeability (61), reduced tensile ductility after long-time aging, and reduced resistance to oxidation. Iron content has relatively small effect on post aging ductility. Manganese content also affects oxidation resistance (see Figures 2.0329 and 2.03210).

1.042 Effect of silicon content on ductility of sheet at room temperature after exposure at 1600 F for 1000 hours, Figure 1.042.

1.05 **Heat Treatment**

1.051 Recommended solution annealing treatments are:

Bar stock and forgings, 2250 F plus water quench;
Plate, 2200 F and water quench; and
Sheet and strip, 2150 to 2200 F and water quench or rapid air cool.

Time at temperature should be approximately 1 hour per inch of thickness but at least 15 minutes (62).

1.052 Rivets should be solution heat treated at 2125 to 2175 F for 10 to 20 minutes followed by water quench or rapid cool (52).

1.053 A moderate amount of cold work followed by aging increases the creep rupture strength at temperatures up to 1800 F. The recommended procedure consists of cold working solution annealed material followed by aging at 900 to 1200 F for 4 to 16 hours, preferably at 1100 F for 4 hours. Appropriate cold reductions are 15 to 45 percent. Higher cold reductions reduce subsequent ductility and are not recommended.

1.06 **Hardness**

1.061 The alloy is primarily hardened by cold work, the effects of which are retained to relatively high temperatures. Solution treating and rapid cooling before cold working leads to an additional moderate increase in strength on aging. The properties in these conditions vary with the carbon content (6).

1.062 Effect of cold reduction and subsequent aging on hardness of sheet, Figure 1.062.

1.063 Effect of cold reduction on hardness of wire, Figure 1.063.

1.064 Effect of cold rolling and aging on hardness of sheet, Figure 1.064.

1.065 Effect of temperature on hot hardness of sheet in cold worked and in cold-worked and aged conditions, Figure 1.065.

1.066 Effect of temperature on hot hardness of bar stock, Figure 1.066.

1.067 Relation between room temperature tensile strength and DPH hardness of sheet, Figure 1.067.

1.07 **Forms and Conditions Available**

1.071 The alloy is available in sheet and plate from 0.025 to 1-inch thickness, in wire and bar from 1/16 to 3-1/2-inch diameter, and in forgings up to 8 inches in diameter (5).

1.072 Wrought products are available in the hot-worked, annealed and cold-worked conditions.

1.073 Precision investment castings are also available.

1.08 **Melting and Casting Practice**

1.081 Standard commercial practice is air induction melt followed by consumable electrode vacuum arc remelt.

1.082 L-605 can also be produced by electroslag remelting (ESR) to comparable cleanliness, compositional uniformity, macrostructure, and mechanical properties as that produced by vacuum arc remelting. The smooth ingot surface and fine grain structure of ESR material allow improved workability and higher ingot-to-billet yield than usually achieved with vacuum-arc-remelt alloy (63).

1.09 **Special Considerations**

1.091 This alloy has been found to embrittle due to the precipitation of Co_2W Laves phase during long-time elevated temperature exposure. This tendency can be reduced by keeping the silicon content below 0.4 percent (24) (in accordance with AMS specifications) or by cold working prior to heat treatment (51). A low temperature age of 10 hours at 700 F after cold working provides a strength increase with minimum sacrifice in elongation (see Figure 3.0215) (61).

1.092 Improvement in oxidation resistance can be achieved by maintaining low manganese content. The higher the silicon content, the lower the manganese content should be to achieve good oxidation resistance. For silicon content from 0.1 to 0.4 percent the preferred range of manganese is between 1.3 and 1.7 percent. See Reference 23 and Figure 2.03210.

1.093 Severe intergranular cracking can occur during fusion welding as a result of inadvertent copper contamination of the surface from contact with copper welding fixtures. The presence of as little as 0.003 mil of

Co
20 Cr
15 W
10 Ni

L-605

copper on the surface of high-cobalt alloys such as L-605 causes liquid metal embrittlement when the local temperature is increased to the melting point of copper, 1981 F. The hot cracks propagate at high velocities once a critical amount of plastic strain is introduced in the weld heat affected zone. Cracks are oriented perpendicular to the principal stress direction. This weld-cracking problem can be alleviated by the use of chromium-plated copper welding fixtures to prevent contact of the workpiece with copper. An alternative solution is to construct welding fixtures of Cu-12A1 or Cu-30Ni, which alloys have been shown to not result in copper contamination cracking of L-605 (64, 65, 66).

1.094 L-605 is subject to nitrogen embrittlement during long-time exposure at elevated temperatures in hydrazine or ammonia atmospheres (see Section 2.035).

2 PHYSICAL PROPERTIES AND ENVIRONMENTAL EFFECTS

2.01 Thermal Properties

2.011 Melting range, 2425 to 2570 F (5).

2.012 Phase changes.

2.0121 A number of carbide and intermetallic phases have been shown to precipitate in L-605 during aging. These include M_7C_3, M_{23},C_6, M_6C, alpha-Co_3W, beta-Co_3W, Laves-Co_2W, and mu-Co_7W_6. The rates of precipitation vary considerably with exposure temperature, as summarized in Figure 2.0121. The order of precipitation at 1470 F is considered to be: (M_7C_3), $M_{23}C_6$, M_6C, Laves-Co_2W, and mu-Co_7W_6. At 1290 F, the order is considered to be: (M_7C_3), M_{23},C_6, M_6C, (alpha-Co_3W), beta-Co_3W, and Laves-Co_2W. The parenthesized phases appear metastable. These two distinctly different orders of precipitation produce differeing age-hardening characteristics and also differing properties. Age-hardening at 1470 F and higher is attributed primarily to precipitation of $M_{23}C_6$, M_6C, and Laves-Co_2W. In contrast, the precipitation of alpha-Co_3W (ordered fcc), which is coherent with the matrix and transforms to beta-Co_3W (ordered hcp) after long-time aging, is important in strengthening the alloy at temperatures below 1290 F. Aging of cold-worked alloy at 1290 F or lower causes preferential precipitation of carbides and beta-Co_3W on stacking faults and on an epsilon phase (hcp, stoichiometry not reported) introduced during cold working. This preferential precipitation causes considerable subsequent age hardening. At higher temperatures (above about 1470 F), disappearance of stacking faults and recrystallization of the matrix result in softening of the alloy (67).

2.0122 Time-temperature-transformation diagram, Figure 2.0122.

2.013 Thermal conductivity, Figure 2.0123.

2.014 Thermal expansion, Figure 2.0214.

2.015 Specific heat 0.092 Btu/lb F (5), 0.090 Btu/lb F (62).

2.016 Thermal diffusivity.

2.02 Other Physical Properties

2.021 Density, 0.330 lb/cu³ in., 9.13 grams/cm³ at room temperature (5).

2.0211 Effect of test temperature on density, Figure 2.0211.

2.022 Electrical properties.

2.0221 Electrical resistivity, 34.9 microhm-inch (5).

2.0222 Electrical resistivity of cold-worked L-605 at low temperatures, Figure 2.0222.

2.023 Magnetic properties. Alloy is nonmagnetic.

2.024 Emittance, Figure 2.024.

2.025 Damping capacity.

2.03 Chemical Environments

2.031 Corrosion.

2.0311 Corrosion rates in severe aqueous media, Table 2.0311.

2.032 Oxidation.

2.0321 L-605 forms a protective oxide scale during exposure to air at elevated temperatures. The oxidation weight gain kinetics in still air are approximately parabolic with time, as shown in Figure 2.0322. Minor deviations from linearity in these log-log plots are attributed to the heterogeneous nature of the oxidation process. At 2200 F, catastrophic oxidation occurs with the formation of a low-melting-point scale containing $CoWO_4$, CoO, and $CoCr_2O_4$. A summary of the external and internal oxides which form during air oxidation of L-605 is shown in Figure 2.0323. The effects of internal oxidation are at least as severe as those caused by conversion of metal to oxide at the surface. Significant subsurface intergranular oxidation occurs which, along with depletion of strengthening constituents such as tungsten and physical reduction in thickness due to external oxidation, also reduces the load-carrying ability of the substrate. As seen in Table 2.0324, the total depth of metal affected increases slowly with time up to 10,000 hours at 1830 F.

Thermal cycling and increased air velocity over the specimens (as encountered in burner rig tests and in service) both act to increase the extent of surface oxidation through spalling, as shown in Figures 2.0325 and 2.0326. However, the total depth of metal affected is relatively unchanged by these variables, as seen by comparison of the data in Figure 2.0327 and Table 2.0324. The depth of metal affected has been observed to be less at an air pressure of 0.16 psi (8 torr) (Figure 2.0328), than at atmospheric pressure (Table 2.0324).

Fatigue properties at room temperature and 1400 F are reduced by prior air exposure (oxidation) at 1800 to 2100 F as shown in Figures 3.053 and 3.054.

2.0322 Oxidation weight gain as a function of time for L-605 in still air at 1400 to 2200 F, Figure 2.0322.

2.0323 Schematic summary of L-605 oxidation process, Figure 2.0323.

2.0324 Long-time oxidation in still air, Table 2.0324.

2.0325 Oxidation weight changes during cyclic furnace and burner rig exposures at 2000 F for L-605, Figure 2.0325.

2.0326 Calculated metal losses after cyclic furnace and burner rig oxidation exposures at 1900 to 2100 F for L-605, Haynes Alloy No. 188, and Hastelloy X, Figure 2.0326.

2.0327 Dynamic oxidation of L-605 after 100 hours at 1600 to 1900 F, Figure 2.0327.

2.0328 Oxidation behavior at 1800 F and air pressure of 0.16 psi (8 torr), Figure 2.0328.

2.0329 Effect of silicon and manganese content on oxidation of sheet in air at 1832 F, Figure 2.0329.

2.03210 Effect of silicon and manganese content on oxidation resistance and post-aging ductility, Figure 2.03210.

2.033 Hot corrosion.

2.0331 The presence of salt in the combustion air and sulfur contaminant in the fuel causes accelerated oxidation at elevated temperatures, termed hot corrosion. The hot corrosion resistance of L-605 as compared to other cobalt-base alloys is shown in Figure 2.0332. L-605 is superior to WI-52, but less corrosion resistant than the cast alloys MAR-M-509, MAR-M-302, and X-40. All of these alloys exhibit internal sulfidation below the oxide/metal interface. The sulfides are of the general form CrS_x, where x varies from 1 to 1.5 depending on the alloy and the test parameters (68). The hot corrosion resistance of L-605 is inferior to that of other sheet superalloys as shown in Figure 2.0333, possibly attributable to the high tungsten content (15 percent) of L-605 (69).

2.0332 Dynamic hot corrosion of L-605 and four other cobalt-base alloys at 1600 to 1900 F, Figure 2.0332.

2.0333 Dynamic hot corrosion of L-605 and other sheet superalloys after 200 hours at 1650 F, Figure 2.0333.

2.034 Hydrogen embrittlement.

2.0341 L-605 is embrittled by hydrogen exposure at 1200 F in the cold-worked condition but not in the solution annealed condition. As shown in Table 2.0342, exposure of 25 percent cold-worked alloy for 100 or 1000 hours in hydrogen at 1200 F causes premature brittle failure on subsequent tensile testing at room temperature. In contrast, solution annealed material exhibits similar ductility after both hydrogen exposure and air exposure at 1200 F (70). [The relatively low ductility of this solution annealed and aged material is attributed to its high silicon content (see Figure 1.042)].

2.0342 Effect of hydrogen exposure at 1200 F on room temperature strength and ductility, Table 2.0342.

2.035 Nitrogen embrittlement.

2.0351 L-605 is subject to nitrogen embrittlement in monopropellant hydrazine (N_2H_4) thrusters to the extent that it is useful only for limited times as a catalyst bed containment screen material. L-605 screens become embrittled and crack, typically after about 10^5 pulses at a maximum catalyst bed temperature of 1800 F, compared to a desired lifetime of 10^6 pulses. The failure mechanism is believed to be progressive growth of thermal fatigue cracks formed in the brittle nitrided surface layer (71).

2.0352 The effects of exposure to ammonia (a hydrazine decomposition product) at 1800 F on the tensile properties of L-605 have been evaluated in order to assess the compatability of L-605 with hydrazine monopropellant for space shuttle applications. Ammonia exposures for 10 or 100 hours at 1800 F increase the strength but reduce ductility of L-605 at 1800 F, as shown in Figure 3.03120. Subsurface hardening indicated that internal nitriding was responsible for the change in tensile properties (72).

Based on these data, L-605 is not attractive for long-time applications involving hydrazine at 1800 F.

2.036 Liquid metal corrosion.

2.0361 The rate of corrosion of L-605 by mercury, shown in Figure 2.0362, is high compared to rates determined for refractory metal alloys (not shown). L-605 is thus relatively unattractive for use in mercury-containing heat transfer loops.

2.0362 Maximum penetration rate of mercury in thermal convection, two-phase loops, Figure 2.0362.

3 MECHANICAL PROPERTIES

3.01 Specified Mechanical Properties

3.011 Specified mechanical properties at room temperature, Table 3.011.

3.012 AMS 5537 specifies that sheet up to and including 0.050-inch thickness shall be capable of bending 180° over a bend radius 1.5 times nominal thickness, and sheet exceeding 0.050-inch thickness shall be capable of bending 120° over a bend radius 2 times nominal thickness, without cracking.

3.013 AMS 5759 specifies that hardness should not be greater than 248 BHN for forgings, not greater than 275 BHN for bars, and not greater than 302 BHN for flash welded rings.

3.014 AMS 5537 and 5759 specify that rupture life at 1500 F and 24 ksi shall not be less than 24 hours with elongation not less than 10 percent.

3.02 Mechanical Properties at Room Temperature

3.021 Tension—stress-strain diagrams—tension properties.

3.0211 Effect of cold reduction on tensile properties of 0.125-inch wire, Figure 3.0211.

3.0212 Effects of cold rolling and cold rolling plus 900 F aging on tensile properties at room temperature, Figure 3.0212.

3.0213 Cold working prior to exposure at 1600 F reduces preferential grain boundary precipitation of hardening phases and promotes more uniform precipitation by providing a greater number of nucleation sites. This more uniform precipitation results in a modest increase in room temperature tensile ductility (see Figure 3.0214) (73).

3.0214 Effect of cold reduction on tensile properties after prior exposure to 1600 F, Figure 3.0214.

3.0215 Effects of aging or annealing on room temperature tensile properties of cold rolled bar, Figure 3.0215 [(a) cold rolled 25 percent, (b) cold rolled 40 percent].

3.022 Compression—stress-strain diagrams—compression properties.

3.023 Impact.

3.0231 Effects of aging at elevated temperatures on notch-impact energy at room temperature, Figure 3.0231.

3.0232 Aging time-temperature curves for 25, 50, and 75 percent reductions in notch-impact energy at room temperature, Figure 2.0232.

3.0233 Dimple, spall, and perforation characteristics of thin sheet, which are of interest for space power system radiator shielding from hypervelocity meteoroid impact, are discussed for L-605 and other candidate materials in Reference 74.

3.024 Bending.

3.0241 Effect of aging time and temperature on embrittlement of sheet as determined by a 1.5 T bend test, Figure 3.0241.

3.025 Torsion and shear.

3.026 Bearing.

3.027 Stress concentration.

3.0271 Notch properties.

3.02711 Notched tensile strength of cold worked and cold worked plus aged bar at room temperature, Table 3.02711.

Co
20 Cr
15 W
10 Ni

L-605

Co
20 Cr
15 W
10 Ni
L-605

3.0272 Fracture toughness.
3.028 Combined properties.

3.03 **Mechanical Properties at Various Temperatures**
3.031 Tension—stress-strain diagrams—tension properties.
3.0311 L-605 exhibits a pronounced tensile ductility minimum in the vicinity of 1400 F. This ductility minimum is attributed to a change in crack propagation mode with increasing temperature from transgranular to intergranular. At temperatures below the ductility minimum, deformation and crack propagation are transgranular and total elongation to fracture is high. However, as the ductility minimum is approached temperature-wise, transgranular deformation is interrupted by intergranular cracking. Wedge-shaped voids produced at triple junctions by grain boundary shear grow unhindered, leading to intergranular failure and a drastic reduction in total elongation at the ductility minimum. At temperatures above the ductility minimum, fracture still occurs by transgranular deformation and grain boundary shear, but thermal recovery causes blunting of crack tips and results in greatly improved ductility (see Figure 3.0314).

After long-time aging at 1500 F [e.g., 11,000 hours (see Figure 3.0318)], copius precipitate (measured as high as 14.7 weight percent), predominantly Co_2W Laves phase, forms at grain and twin boundaries and as well-distributed bulky particles and platelets within the grains. At low temperatures, grain boundary precipitates induce early intergranular fracture of the aged material, causing low tensile ductility. However, at about 1400 to 1500 F, corresponding to the ductility minimum for solution annealed material, high elongation is observed in aged material. The fracture mode changes to transgranular. This ductility increase is attributed to several factors: (1) transgranular deformation is enhanced and crack tips blunted by a more plastic matrix softened by solute depletion; (2) brittle precipitate phases become tougher and more resistant to cracking with increasing temperature; and (3) intragranular precipitate particles dispersed near the grain boundaries reduce grain boundary shear and inhibit intergranular crack propagation (75).

3.0312 Stress-strain curves for 0.063-inch sheet at room and elevated temperatures at several strain rates, Figure 3.0312.
3.0313 Stress-strain curves for 0.109 and 0.040-inch sheet at room and elevated temperatures at several strain rates, Figure 3.0313.
3.014 Effect of test temperatures on tensile properties of bar and sheet, Figure 3.0314.
3.015 Effect of test temperature and strain rate on tensile and yield strength of sheet, Figure 3.0315.
3.016 Typical effects of test temperature and strain rate on tensile properties of sheet, Figure 3.0316.
3.0317 Effect of test temperature on tensile properties of cast bar in solution treated condition, Figure 3.0317.
3.0318 Effect of test temperature on tensile properties of sheet after 11,000-hour exposure at 1500 F, Figure 3.0318.
3.0319 Effect of low test temperatures on tensile and yield strength of sheet, Figure 3.0319.
3.03110 Effect of low temperature on tensile elongation of sheet, Figure 3.03110.
3.03111 Effect of test temperature and strain rate on tensile properties of 20 percent cold-worked sheet, Figure 3.03111.
3.03112 Effect of test temperature and strain rate on tensile properties of 10 percent cold-worked and aged sheet, Figure 3.03112.
3.03113 Effects of cold rolling and cold rolling plus 1450 F aging on tensile properties at 1450 F, Figure 3.03113.
3.03114 Effect of test temperature on tensile properties of as-cold-worked sheet, Figure 3.03114.
3.03115 Effect of test temperature on tensile properties of cold-worked and aged sheet, Figure 3.03115.
3.03116 Effect of test temperature on tensile properties of cold-worked and shot-peened sheet, Figure 3.03116.
3.03117 Effect of test temperature on tensile properties of cold-worked, shot-peened and aged sheet, Figure 3.03117.
3.03118 Effect of test temperature on tensile properties of cast bar when solution treated, stress relieved and aged, Figure 3.03118.
3.03119 Effect of aging time and temperature on elevated temperature tensile properties of vacuum arc-melted bar, Figure 3.03119.
3.03120 Tensile properties of L-605 at 1800 F after exposure to partially dissociated ammonia at 1800 F, Figure 3.03120.
3.032 Compression—stress-strain diagrams—compression properties.
3.0321 Stress-strain curves in compression for sheet at room and elevated temperatures at several strain rates, Figure 3.0321.
3.0322 Typical effects of test temperature and strain rate on compressive yield strength, Figure 3.0322.
3.033 Impact.
3.0331 Effect of test temperature on impact strength of plate, Figure 3.0331.
3.0332 Effect of low temperature on impact strength of solution treated or solution treated and cold rolled plate, Figure 3.0332.
3.0333 Effects of aging at elevated temperatures on notch-impact energy at 570 F, Figure 3.0333.
3.034 Bending.
3.035 Torsion and shear.
3.0351 Effect of test temperature on shear strength of sheet, Figure 3.0351.
3.0352 Effect of test temperature on shear strength of plate and forging, Figure 3.0352.
3.036 Bearings.
3.0361 Effect of test temperature on bearing ultimate and yield strengths, Figure 3.0361.
3.037 Stress concentration.
3.071 Notch properties.
3.0372 Fracture toughness.
3.038 Combined properties.

3.04 **Creep and Creep-Rupture Properties**
3.041 Creep-rupture curves for bar at temperatures from 1200 to 1800 F for times up to 40,000 hours, Figure 3.041.
3.042 Stress required to produce total plastic strains of 0.5 and 1.0 percent at 1200 and 1500 F, Figure 3.042.
3.043 Weibull distribution of creep-rupture life for bar and forgings at 1500 F and 24 ksi, Figure 3.043.
3.044 Creep-rupture strength at elevated temperatures, Figure 3.044.

3.045 Minimum creep-rate curves for bar at 1200 and 1500 F, Figure 3.045.

3.046 Creep strength at elevated temperatures, Figure 3.046.

3.047 Very long time creep curves for bar at 1200 and 1500 F, Figure 3.047.

3.048 The creep behavior of seamless tubes of L-605 has been evaluated. Tubes measuring 0.375-inch outside diameter by 0.025-inch wall were internally pressurized with 600 to 1800 psi helium and tested in air at 1518 to 1700 F. Rupture lives varied from 385 to 4609 hours for tubes from one heat of material and 144 to 1308 hours for tubes from a second heat. The creep rupture life data from the stronger (first) heat of material correlated well with published data on uniaxial creep of L-605, while the data from the second heat indicated strengths which were 20 to 40 percent lower. The lower strength of the second heat was attributed to the presence of longitudinal stringers (observed metallographically). It was concluded that the creep properties of tubes can be calculated accurately from uniaxial creep data, but preferably using data from the same heat of material since creep properties can vary from heat to heat (76).

3.049 Creep crack growth in L-605 occurs over a limited temperature range of about 1200 to 1400 F, with rates as shown in Figure 3.0410. The rate of growth at 1400 F is about five-fold greater than that at 1200 F. At 1600 F (not shown), crack tip blunting and stress relaxation occur faster than nucleation and growth of grain boundary microcracks. Under these conditions, time-dependent crack growth does not occur. At temperatures below 1200 F, creep rates are sufficiently slow so as to minimize the grain boundary damage process that is a prerequisite for creep crack growth. Creep crack growth is proposed to occur by the nucleation and growth of wedge-type cracks at triple point junctions due to grain boundary sliding or by the formation and growth of cavities at the boundaries (77).

3.0410 Creep crack growth at elevated temperatures, Figure 3.0410.

3.0411 Torsional stress relaxation at elevated temperatures, Table 3.0411.

3.0412 Stress relaxation of wire at 600 F, Figure 3.0412.

3.05 **Fatigue**

3.051 Room temperature fatigue of sheet and bar in axial loading, Figure 3.051.

3.052 Reversed strain cycling fatigue of hollow tube at 1000 and 1200 F, Figure 3.052.

3.053 Fatigue of thin sheet at room temperature after 100-hour cyclic air exposures at 1800 to 2100 F, Figure 3.053.

3.054 Fatigue of thin sheet at 1400 F after 100-hour cyclic air exposures at 1800 and 2000 F, Figure 3.054.

3.055 Low cycle fatigue crack growth at elevated temperatures, Figure 3.055.

3.056 L-605 has superior fatigue crack-growth properties as compared to Inconel X-750, Inconel 718, and Incoloy 800 at 800 to 1300 F, as shown in Figure 3.057.

3.057 Stress intensity factor range as a function of temperature for fatigue crack growth in L-605 and three other high temperature alloys, Figure 3.057.

3.06 **Elastic Properties**

3.061 Poisson's ratio, Figure 3.061.

3.062 Modulus of elasticity.

3.0621 Modulus of elasticity in tension, Figure 3.0621.

3.0622 Modulus of elasticity of sheet in compression, Figure 3.0622.

3.0623 Dynamic modulus at room and elevated temperatures, Figure 3.0623.

3.063 Modulus of rigidity, Figure 3.063.

3.064 Tangent modulus.

3.065 Secant modulus.

Co
20 Cr
15 W
10 Ni

L-605

4 FABRICATION

4.01 **Forming**

4.011 General. Although this alloy has excellent ductility in the annealed condition, the power requirements for cold forming are high and frequent intermediate anneals are needed during severe forming because of the high rate of strain hardening (7). Heating to a temperature of 450 F can be used advantageously for forming sheet and other products. Detailed information on formability limits for different processes can be found in (42, 43, 44).

4.012 Uniform elongation and total elongation for 8 inches gage length of sheet deformed in tension to simulate forming operation at room temperature and 450 F, Figure 4.012.

4.013 Erichsen cup test data for cold-reduced L-605, Table 4.013.

4.014 The use of a glass lubricant can significantly reduce power requirements during warm rolling. Heated rolls of a stiff alloy such as IN-100 also reduce roll separating force (see Table 4.015) (78).

4.015 Warm rolling with heated rolls or with lubricant, Table 4.015.

4.016 The forging starting temperature should be no greater than 2200 F and finishing temperature no less than 1800 F. The forging temperature should be high enough to minimize grain boundary carbides and low enough for grain size control. The optimum forging temperature is approximately 2150 F. Silicon content should be held to a maximum of 0.25 percent for optimum fabricability. The minimum temperature is dependent upon the nature and degree of working. In forging use light rapid blows until the cast structure is refined. Do not attempt to change the general shape of an ingot, as from square to round, during the initial stages of forming to avoid corner cracks; forging can be cooled at any desired rate (5,7). Neutral or slightly oxidizing atmosphere should be used for preheating. Soaking time should be about 1 hour per inch of thickness prior to hot working (62).

4.02 **Machining and Grinding**

4.021 General. Machinabiltiy of this alloy is best in the annealed condition, with a hardness of about 225 BHN or 20 HRC, although cold worked material with hardnesses up to 50 HRC are also machinable. The same techniques used for austenitic stainless steels are suitable. Very sharp tools, preferably cemented carbide tools, positive cuts, slow feeds and speeds, and rigid equipment should be used. A good commercial soluble oil is satisfactory as coolant and lubricant (5).

4.022 Finish of the part is improved by using high speeds and slow feeds. The finish attainable with cold-worked material is superior to that with annealed material.

Co
20 Cr
15 W
10 Ni
L-605

4.03 **Joining**

4.031 General. The alloy can be joined by most fusion and resistance welding methods and by brazing.

4.032 Fusion welding can be performed manually or automatically by the inert gas arc welding method with a minimum of heat input using either tungsten or consumable L-605 electrodes. For manual arc welding coated L-605 electrodes are available. The Sigma method is also suitable. Submerged welding is not recommended because this procedure is characterized by high heat input to the base metal and slow cooling of the weld and may result in large grains and embrittlement. It is advisable to fusion weld in the solution annealed condition rather than the cold-worked condition.

Careful edge preparation is required to assure good welds. Machining of edges is best to obtain correct fits, although hand grinding is satisfactory. Thermal cutting, except by Heliarc, is not recommended. Restraint during welding should be kept at a minimum and welding from both sides is recommended wherever possible. When this is not practical, the joint spacing should be increased and a copper backing bar used (see precautions with regard to use of copper in Section 1.093). Currents slightly higher than normal are then used to obtain complete penetration. Direct current with reversed polarity produces the best mechanical properties. Whenever possible, welding should be done in the flat position. Rapid cooling after welding is recommended, as well as post-weld annealing, to prevent or eliminate any embrittlement which may have occurred between 1400 and 1800 F (5,8).

4.033 Effect of test temperature on tensile properties of unwelded and butt-welded sheet, Figure 4.033.

4.034 Effect of low test temperature on tensile strength of GTA welded sheet, Figure 4.034.

4.035 Tensile strength of brazed T-joints at room and elevated temperatures, Table 4.035.

4.04 **Surface Treating**

4.041 The tightly adhering oxide scale which forms during air annealing can be removed by blasting with abrasive or by treatment in molten caustic followed by acid pickling. A suitable procedure for caustic/acid pickling is as follows:

1. Dip in sodium hydride (caustic) at 700 F for 15 minutes;
2. Dip in sulfuric acid (8 to 12 percent) at 140 to 160 F for 10 to 15 minutes; and
3. Dip in mixture of nitric acid (12 to 15 percent) plus hydrofluoric acid (1 to 3 percent) at 125 to 160 F for 15 minutes.

The material should be thoroughly rinsed in water after each operation (62).

REFERENCES

1 AMS 5537D (October 15, 1979).
2 AMS 5759F (January 15, 1980).
3 AMS 5796A (October 15, 1980).
4 AMS 5797A (July 16, 1979).
5 Haynes Stellite Company, "Haynes Alloy No. 25" (March 1959).
6 Westinghouse Electric Corporation, "Properties of Haynes Alloy No. 25 (L-605)", Bettis Plant Materials Manual (May 1957).
7 Universal Cyclops Steel Corporation, "High Temperature Metals, Unitemp L-605" (1959).
8 General Electric Company, Small Aircraft Engine Department, Cobalt Alloy Materials Handbook (April 15, 1959).
9 Roe, William P. and Kattus, J. R., "Tensile Properties of Aircraft Structural Metals at Various Rates of Loading after Rapid Heating", TR-55-199, Part III, Wright Air Development Center (September 1957).
10 ASTM, "Report on the Elevated Temperature Properties of Selected Super Strength Alloys", Special Technical Publications No. 160 (1954).
11 Wade, William R., "Measurements of Total Hemispherical Emissivity of Several Stably Oxidized Metals and Some Refractory Oxide Coatings", NASA Memo 1-20-59L, National Aeronautics and Space Administration (January 1959).
12 Morrison, Joseph and Kattus, J. R., "Tensile Properties of Aircraft Structural Metals at Various Rates of Loading after Rapid Heating", TR-55-199 Part II, Wright Air Development Center (November 1956).
13 AF-TR 6731, Part I (1952).
14 General Electric Company, "L-605 Sheet—0.2 Percent Plastic Creep", 4012222-144 (October 6, 1956).
15 General Electric Company, L-605 Sheet—Master Rupture, A-4012220-145 (October 6, 1956).
16 General Electric Company, L-605—Physical Properties, A-4012220-503 (February 23, 1959).
17 Cryogenics Materials Data Handbook, Air Force Materials Laboratory Report, ML-TDR-64-280 (August 1964).
18 Materials Properties Handbook, NATO, AGARD, Engineering Sciences Data Unit of Royal Aeronautical Society, Vol. IV, Heat Resisting Alloys.
19 Arp, V., et al., "Thermal Expansion of Some Engineering Materials from 20 to 293 K", Cryogenics, Vol. 2, No. 4 (June 1962).
20 Watson, J. F., et al., "Selection of Materials for Cryogenic Applications in Missiles and Aerospace Vehicles", MRG—132 Convair/Astronautics (February 1960).
21 Mikesell, R. P. and Reed, R. P., "The Impact Testing of Various Alloys at Low Temperatures", Advances in Cryogenic Engineering, Plenum Press, New York, Vol. 3 (1957), p 316.
22 Warren, K. A. and Reed, R. P., "Tensile and Impact Properties of Selected Materials from 20 to 300 F", Monograph 63, National Bureau of Standards (June 1963).
23 Wolf, James S. and Sandrock, Gary D., "Some Observations Concerning the Oxidation of the Cobalt-Base Superalloy L-605 (HS-25)", NASA TND-4715 (August 1968).
24 Sandrock, Gary D., Ashbrook, Richard L., and Freche, John C., "Effect of Variations in Silicon and Iron Content on Embrittlement of a Cobalt-Base Alloy (L-605)", NASA TN D-2989 (September 1965).
25 Badger, F. S., "Superalloys for Airframe Structures", Metal Progress Vol. 71, No. 6 (1957), p 109.

26 Hanschka, R. M., "Engineering Properties of High Strength to Weight Alloys and Super Alloys for Aircraft and Missile Applications", Materials and Process Applications Section, Wright Aeronautical Division (January 18, 1963).

27 Popp, H. E., "Materials Property Data Compilation", Third Quarterly Report, General Electric Company, Large Jet Engine Department (November 1, 1962).

28 Haynes Stellite Company, "Haynes Alloy No. 25", (September 1960).

29 Engineering Alloy Digest, HS 25, High Temperature Spring Data Sheet (June 1961).

30 Dioguardo, P. R. and Lloyd R. D., "Investigation of the Effects of Rapid Properties of Compressive and Column Members", The Marquardt Corporation, ASD-TR 61-499 (January 1962).

31 Haynes Stellite Company, "Haynes Alloy No. 25", (June 1962).

32 Baughman, R. A., "Gas Atmosphere Effects on Materials", General Electric Company, WADC Technical Report 59-511 (May 1960).

33 Claus, J., Meredith, D., and Sutch, F., "Manufacturing Methods for Hot Structures", Boeing Airplane Company, AMC-TR 60-7-795, Section I, Vol. I (December 1960).

34 Dukes, W. H., Gosden, G. E., Kappelt, G. F., and Mirti, A. E., "Manufacturing Methods for Insulated and Cooled Double-Wall Structures", Bell Aerospace Company, ASD-TR 61-7-799, Section I (II) (May 1961).

35 Lieberman, W. and Rowe, G. H., "High Temperature Strength Properties of Commercial and Vacuum Melted Haynes Alloy No. 25", Pratt and Whitney Report PWAC-351 (June 21, 1961).

36 Wood, W. W., et al., "Sheet Metal Forming Technology", Chance Vought Corporation (Aeronautics and Missiles Division), ASD-TR-7-871 (III) (September 1962).

37 Morris, G. A., "Formability Characteristics of L-605", McDonnell Aircraft Corporation Report No. 8880, Serial No. 7 (July 10, 1962).

38 Bernett, E. C., "Tensile Properties of Haynes 25 (L-605) Alloy Sheet", The Marquardt Aircraft Company, Report No. MP 48 (November 19, 1958).

39 Morrison, J. D. and Kattus, J. R., "Tensile Properties of Aircraft Structural Metals at Various Rates of Loading after Rapid Heating", Southern Research Institute, WADC TR-55-199, Part II (November 1956).

40 Roe, W. P. and Kattus, J. R., "Tensile Properties of Aircraft Structural Metals at Various Rates of Loading after Rapid Heating", Southern Research Institute, WADC Report TR-55-199, Part III (July 1957).

41 Kattus, J. R., "Tensile Properties of Aircraft Structural Metals at Various Rates of Loading after Rapid Heating", Southern Research Institute, WADC Report TR 58-440, Part II (February 1959).

42 Strohecker, D. E., Byrer, T. G., Gerds, A. F., Gehrki, J. A., and Boulger, F. W., "Deformation Processing of Nickel Base and Cobalt Base Alloys", NASA-TMX 53439 (April 18, 1966).

43 Wood, W. W., et al., "Final Report on Sheet Metal Forming Technology, Volumes I, II," Aeronautics and Missiles Division, Chance Vought Corporation, ASD-TDR-63-71-871 (1963).

44 Wood, W. W., et al., "Theoretical Formability", Volumes I and II, Chance Vought Corporation, ASD-TDR-61-191-I and II (August 1961).

45 Norwood, D. L., "Sheet Formability at Ambient Temperatures", ASM Metals Engineering Quarterly, Vol. 5, No. 1, (February 1965), pp 41-51.

46 Wlodek, S. T., "Embrittlement of a Co-Cr-W (L-605) Alloy", Trans ASM, Vol. 56, No. 3 (1963), pp. 287-303.

47 Greene, A., Sieber, H., Wells, D., and Wolfe, T., "Research Investigation to Determine Mechanical Properties of Nickel and Cobalt Base Alloys for Inclusion in Military Handbook 5", Vol. I, ML-TDR-64-116 (October 1964).

48 Cooper, David B., "Operations of a Forced Circulation, Haynes No. 25, Mercury Loop to Study Corrosion Product Separations Techniques", NASA CR-241 (July 1965).

49 Widmer, R., Dhosi, J. M., Mullendore, A., and Grant, N. J., "Mechanisms Associated with Long Time Creep Results", AFML-TR-65-181, Part II (March 1967).

50 Teledyne Materials Research Company, "Mechanisms Associated with Long-Time Creep Phenomena", Contract No. AF 33(615)-67-C-1543, Summary Technical Report (March 1, 1967 to June 23, 1968).

51 Sandrock, Gary D. and Leonard, L., "Cold Reduction as a Means of Reducing Embrittlement of a Cobalt-Base Alloy (L-605)", NASA TN D-3528 (August 1966).

52 AMS 5797A (July 16, 1979).

53 Blank, H. A., Hall, A. M., Jackson, J. H., Frank, J. W., and Anderson, W. K., "The Heat Treatment and Working of Haynes 25 Alloy", US. AEC, BMI 814 (April 6, 1953).

54 Davis, J. E., Fischler, J. E., Lobbelt, J. W., Saltman, D., Stanwood, J. W., and Tiner, N. A., "Investigation into More Complete Use of Structural Materials through a Study of the Stress-Temperature-Time Conditions of a Re-Entry Vehicle", Douglas Aircraft Company Inc., WADD TR-60-363 (November 1960).

55 Morral, F. R., Habraken, L., Coutsouradis, D., Drapier, J. M., and Urbain, "Microstructure of Cobalt-Base High Temperature Alloys", Technical Report D8-21.1 ASM (October 1968).

56 Manson, S. S. and Halford, G. R., "A Method of Estimating High-Temperature Low-Cycle Fatigure Behavior of Materials", Conference on Thermal and High Strain Fatigue, Monograph and Report Series No. 32, The Metals and Metallurgy Trust, London, England (June 1967).

57 Slunder, C. J., "Short Time Tensile Properties of the Co-20Cr-15W-10Ni Cobalt Base Alloy (L-605)", DMIC Memorandum 179 (September 27, 1963).

58 Newton, E. H., Johnson, D. E., and Sienczyk, J. L., "Metal Filaments for High Temperature Fabrics", Symposium on High Temperature Fibrous Materials, ASD-TDR-62-964 (January 1963).

59 Freeman, L. H., "Liquid-Fuel Rocket Engine for the Space Shuttle", *Tooling and Production*, Vol. 42, No. 10 (January 1977), pp 48-51.

60 Simmons, W. F., "Current and Future Materials Usage in Aircraft Gas Turbine Engines", Battelle Columbus Laboratories, Columbus, Ohio, MCIC-73-14 (June 1973).

Co
20 Cr
15 W
10 Ni

L-605

Co
20 Cr
15 W
10 Ni
L-605

61 Harlow, R. A., "Manufacturing Methods for Producing L-605 Hardware", Marquardt Corporation, Van Nuys, California, AFML TR-67-414 (January 1968).

62 "Unitemp L-605—High Temperature Metal", Universal-Cyclops Steel Corporation, Bridgeville, Pennsylvania (September 1975).

63 Cook, R. L., Reese, G. W., and Gadsby, D. M., "Electroslag Remelting of Nickel Base Alloys", Wallace-Murray Corporation, Lockport, New York, Symposium Proceedings Part I, held at Mellon Institute, Pittsburgh, Pennsylvania (June 8-10, 1971).

64 Matthews, S. J., Maddock, M. O., and Savage, W. F., "How Copper Surface Contamination Affects Weldability of Cobalt Superalloys", *Welding Journal*, Vol. 51, No. 5 (May 1972), pp 326-328.

65 Savage, W. F., Nippes, E. F., and Mushala, M. C., "Liquid-Metal Embrittlement of the Heat-Affected Zone by Copper Contamination', *Welding Journal*, Vol. 57, No. 8 (August 1978), pp 237-s-245-s.

66 Nippes, E. F. and Ball D. J., "Copper-Contamination Cracking: Cracking Mechanism and Crack Inhibitors", *Welding Journal*, Vol. 61, No. 3 (March 1982), pp 75-s-81-s.

67 Yukawa, N., and Sato, K., "The Correlation Between Microstructure and Stress Rupture Properties of a Co-Cr-Ni-W (HS-25) Alloy", *Supplement to Transactions of the Japan Institute of Metals*, Vol. 9 (1968), pp 680-686.

68 Beltran, A. M., "The Oxidation of Hot-Corrosion Resistance of Cobalt-Base Superalloys", *Cobalt*, Vol. 46 (March 1970), pp 3-14.

69 Simmons, J. J. and Wlodek, S. T., "Hot Corrosion Data for High Performance Sheet Alloys", Stellite Division, Cabot Corporation, Kokomo, Indiana, Research and Development Report (May 17, 1974).

70 Gray, H. R., "Embrittlement of Nickel-, Cobalt-, and Iron-Base Superalloys by Exposure to Hydrogen", NASA-Lewis Research Center, Cleveland, Ohio, NASA TN D-7805 (January 1975).

71 Ewing, A. N., Kamber, K. T., Kendall, E. G., and Sherman, R. G., "Environmental Corrosion of L-605 and Improved Monopropellant Catalyst Screen Materials for Low Thrust Rocket Engines", Aerospace Corporation, El Segundo, California, paper presented at the 1974 Triservice Corrosion of Military Equipment Conference, Dayton, Ohio (October 29-31, 1974).

72 Marcy, R. D., "Material Evaluation Program, High-Temperature Nitriding Environment", Rockwell International Corporation, Canoga Park, California, NASA CR-144382 (October 1973).

73 Sandrock, G. D. and Andrews, C. W., "Effects of Cold Work and Aging on the Substructure and Precipitation Phenomena in the Cobalt-Base Alloy L-605", NASA-Lewis Research Center, Cleveland, Ohio, NASA TN D-7051 (February 1971).

74 Clough, N., Lieblein, S., and McMillan, A. R., "Dimple, Spall, and Perforation Characteristics of Thin Plates of Nine Materials under Hypervelocity Impact", NASA-Lewis Research Center, Cleveland, Ohio, NASA TN D-5625 (January 1970).

75 Hammond, J. P., "Ductility Minimum and Its Reversal with Prolonged Aging in Cobalt- and Nickel-Base Superalloys", Oak Ridge National Laboratory, Oak Ridge, Tennessee, paper presented at the ASME Meeting, San Francisco, California (December 10, 1978).

76 Gumto, K. H., "Creep-Rupture Tests of Internally Pressurized Haynes Alloy No. 25 Tubes", NASA-Lewis Research Center, Cleveland, Ohio, NASA TM X-2346 (August 1971).

77 Sadananda, K. and Shahinian, P., "Creep Crack Growth Behavior of Several Structural Alloys", *Metallurgical Transactions*, Vol. 14A (July 1983), pp 1467-1480.

78 Popoff, A. A., Byrer, T. G., and Fiorentino, R. J., "Studies on the Application of the Heated-Roll Concept to Hot Rolling Metals", Battelle Columbus Laboratories, Columbus, Ohio, Final Report, N00019-69-C-0288 (June 30, 1970).

79 Papadakis, E. P., "Tabulation of the Coefficients of a Quadratic Function for the Thermal Expansion of Various Alloys and Other Engineering Materials", *Materials Science and Engineering*, Vol. 10 (1972), pp 195-203.

80 Clark, A. F., Childs, G. E., and Wallace, G. H., "Electrical Resistivity of Some Engineering Alloys at Low Temperatures", *Cryogenics*, Vol. 4 (August 1970), pp 295-305.

81 Uhlig, H. H., "Passivity in Metals and Alloys", *Corrosion Science*, Vol. 19, No. 11 (1979), pp 777-791.

82 Wasielewski, G. E. and Rapp, R. A., "High-Temperature Oxidation", The Superalloys, edited by C. T. Sims and W. C. Hagel, John Wiley and Sons, New York (1972), pp 287-316.

83 Angerman, C. L., "Long-Term Oxidation of Superalloys", *Oxidation of Metals*, Vol. 5, No. 2 (November 1972), pp 149-167.

84 Barrett, C. A., Johnston, J. R., and Sanders, W. A., "Static and Dynamic Cyclic Oxidation of 12 Nickel-, Cobalt-, and Iron-Base High-Temperature Alloys", *Oxidation of Metals*, Vol. 12, No. 4 (August 1978), pp 343-377.

85 Simmons, J. J. and Wlodek, S. T., "Dynamic Oxidation Data for High Performance Sheet Alloys", Stellite Division, Cabot Corporation, Kokomo, Indiana, Research and Development Report (May 17, 1974).

86 Royster, D. M. and Lisagor, W. B., "Effect of High-Temperature Creep and Oxidation on Residual Room-Temperature Properties for Several Thin-Sheet Superalloys", NASA-Langley Research Center, Langley Station, Virginia, NASA TN D-6893 (November 1972).

87 McCoy, H. E. and Bourgette, D. T., "Influence of Aging on the Impact Properties of Hastelloy N, Haynes Alloy No. 25 and Haynes Alloy No. 188", Union Carbide Corporation, Oak Ridge, Tennessee, ORNL-TM-4380 (December 1973).

88 Hammond, J. P., "Effect of Long-Term Aging at 815 C on the Tensile Properties and Micrstructural Stability of Four Cobalt- and Nickel-Base Superalloys", Union Carbide Corporation, Oak Ridge, Tennessee, ORNL-5174 (August 1976).

89 Moon, D. P., Simon, R. C., and Favor, R. J., "The Elevated-Temperature Properties of Selected Superalloys", Battelle Columbus Laboratories, Columbus, Ohio, ASTM DS-7-S1 (July 1968).

90 Manjoine, M. J. and Voorhees, H. R., "Compilation of Stress-Relaxation Data for Engineering Alloys", ASTM-DS-60 (1982).

91 Malik, R. K. and Stetson, A. R., "Evaluation of Superalloys for Hypersonic Vehicle Honeycomb Heat

Shields", Solar Division of International Harvester Company, San Diego, California, AFML TR-68-292 (October 1968).

92 Shahinian, P., "Fatigue Crack Growth Characteristics of High-Temperature Alloys", *Metals Technology*, Vol. 5, No. 11 (November 1978), pp 372-380.

93 Fritz, L. J. and Koster, W. P., "Tensile and Creep Rupture Properties of (16) Uncoated and (2) Coated Engineering Alloys", Metcut Research Associates, Incorporated, Cincinnati, Ohio, NASA CR-135138 (January 15, 1977).

94 Faulkner, W. H., "Mechanical Properties of Production Cold-Rolled Haynes Alloy No. 25 Sheet", Haynes Stellite Company, Kokomo, Indiana, Summary Report (June 16, 1958).

95 Brentnall, W. D., Stetson, A. R., and Metcalfe, A. G., "Joining of Superalloy Foils for Hypersonic Vehicles", Solar Division of International Harvester Company, San Diego, California, AFML TR-68-299 (October 1968).

Co
20 Cr
15 W
10 Ni

L-605

L-605		
Form	AMS	Military
Sheet	5537D	
Bar, Forging, Ring	5759F	
Welding Wire	5796A	MIL-R-5031, C 13
Welding Electrode, Covered	5797A	MIL-E-6844, C 14
Rivets	7236C	

TABLE 1.031. SPECIFICATIONS (1,2,3,4,52)

L-605		
Element	Minimum, percent	Maximum, percent
Chromium	19.00	21.00
Tungsten	14.00	16.00
Nickel	9.00	11.00
Iron	–	3.00
Manganese	1.00	2.00
Silicon	–	0.40(a)
Carbon	0.05	0.15
Phosphorus	–	0.04
Sulfur	–	0.03
Cobalt	Balance	

(a) 1.00 maximum silicon in welding wire (3) and welding electrodes (4).

TABLE 1.041. COMPOSITION (1,2,3,4,52)

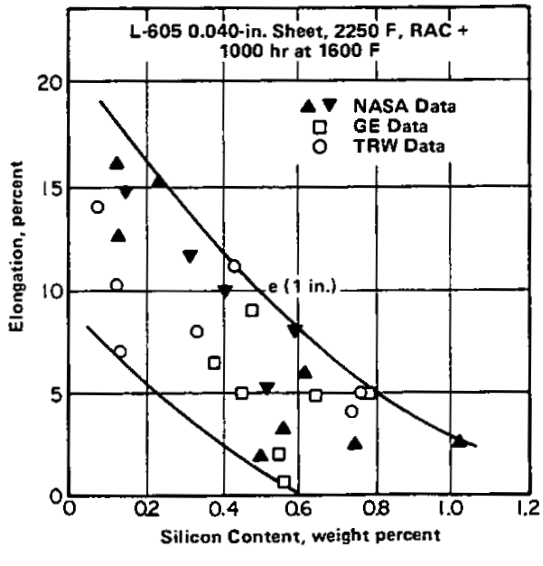

FIGURE 1.042. EFFECT OF SILICON CONTENT ON DUCTILITY OF SHEET AT ROOM TEMPERATURE AFTER EXPOSURE AT 1600 F FOR 1000 HOURS (23)

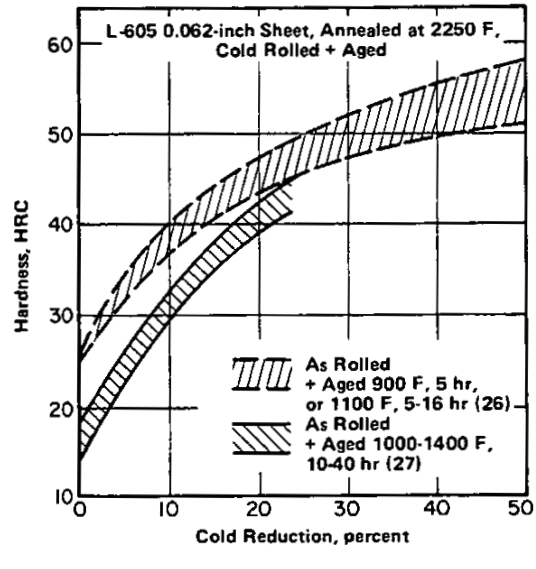

FIGURE 1.062. EFFECT OF COLD REDUCTION AND SUBSEQUENT AGING ON HARDNESS OF SHEET (26,57)

Co
20 Cr
15 W
10 Ni
L-605

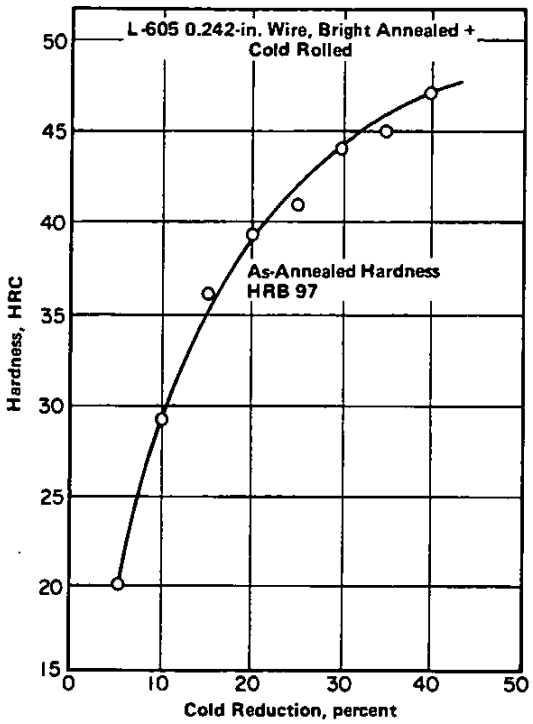

FIGURE 1.063. EFFECT OF COLD REDUCTION ON HARDNESS OF WIRE (28,57)

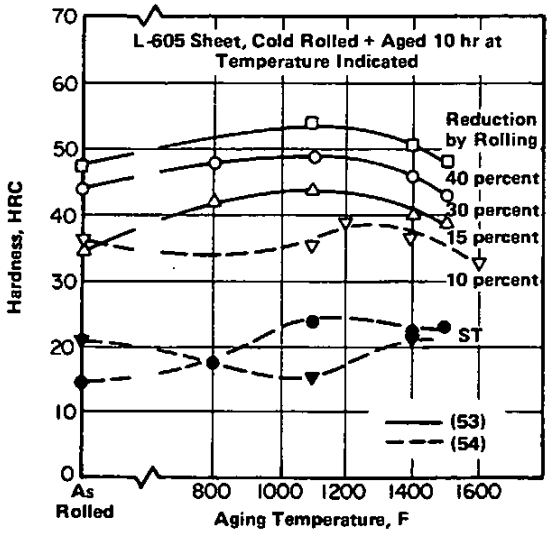

FIGURE 1.064. EFFECT OF COLD ROLLING AND AGING ON HARDNESS OF SHEET (53,54)

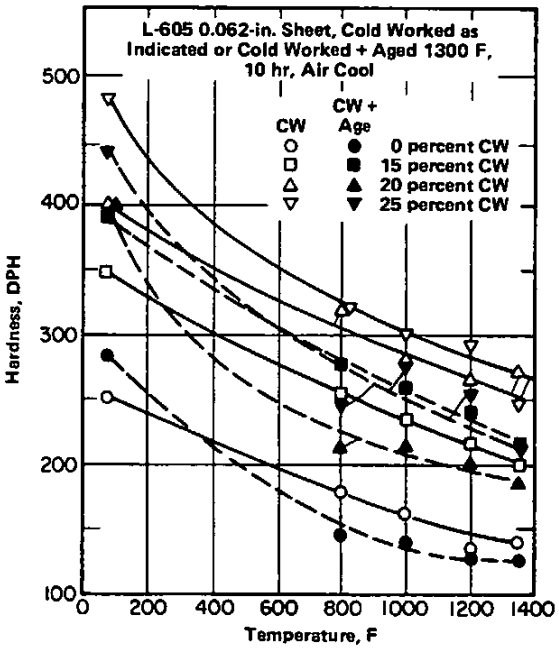

FIGURE 1.065. EFFECT OF TEMPERATURE ON HOT HARDNESS OF SHEET IN COLD WORKED AND IN COLD WORKED AND AGED CONDITIONS (27)

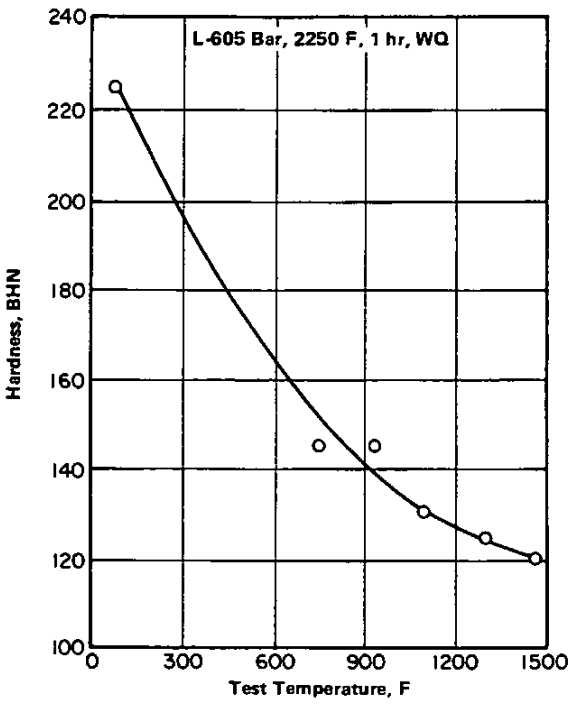

FIGURE 1.066. EFFECT OF TEMPERATURE ON HOT HARDNESS OF BAR STOCK (26)

Co
20 Cr
15 W
10 Ni
L-605

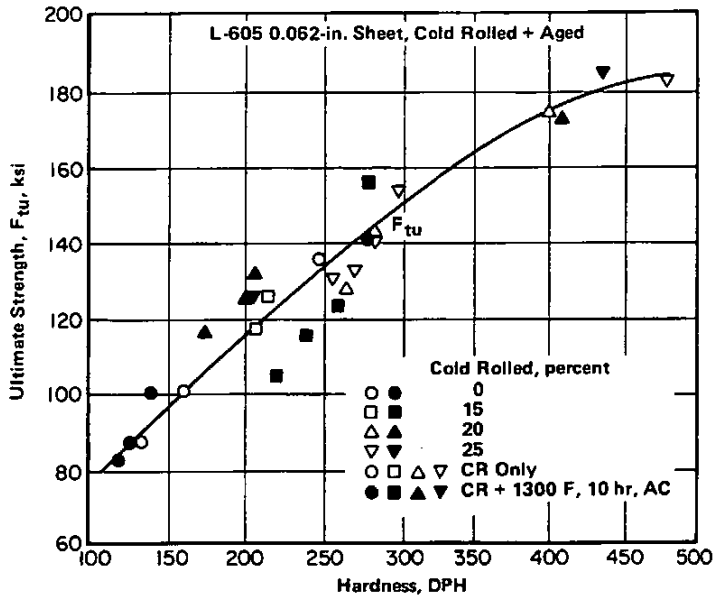

FIGURE 1.067. RELATION BETWEEN ROOM TEMPERATURE TENSILE STRENGTH AND DPH HARDNESS OF SHEET (27)

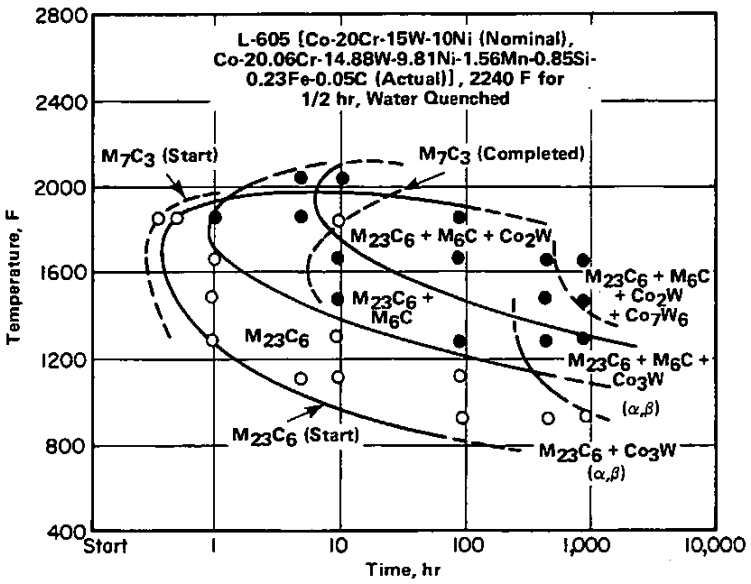

FIGURE 2.0122. TIME-TEMPERATURE-TRANSFORMATION DIAGRAM (55)

Co
20 Cr
15 W
10 Ni
L-605

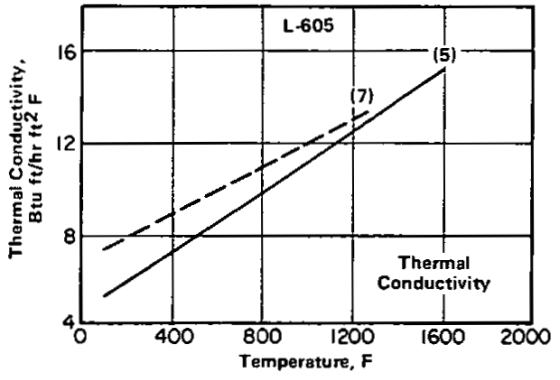

FIGURE 2.013. THERMAL CONDUCTIVITY (5,7)

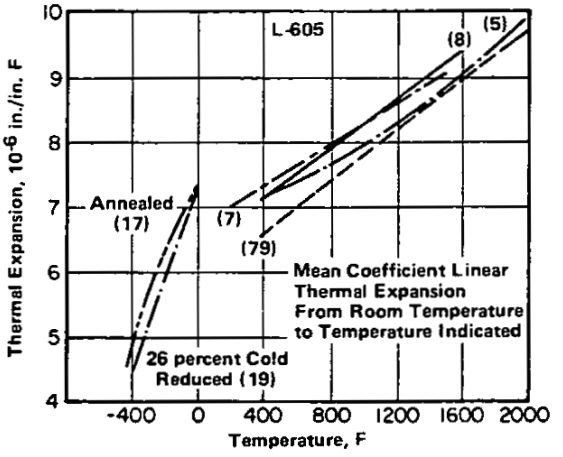

FIGURE 2.014. THERMAL EXPANSION (5,7,8,17,19,79)

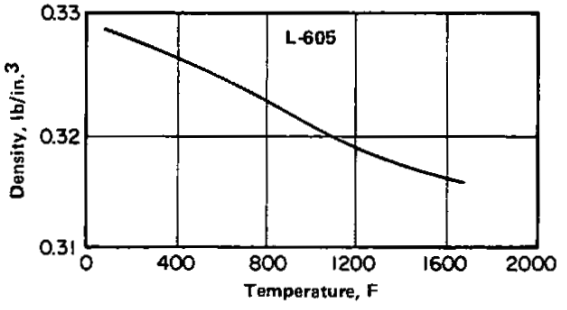

FIGURE 2.0211. EFFECT OF TEST TEMPERATURE ON DENSITY (18)

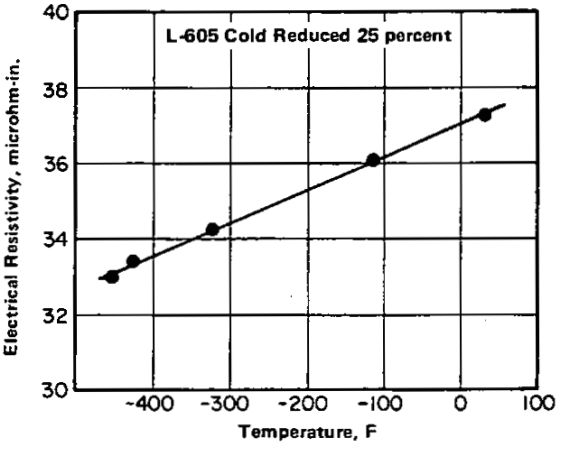

FIGURE 2.0222. ELECTRICAL RESISTIVITY OF COLD WORKED L-605 AT LOW TEMPERATURES (80)

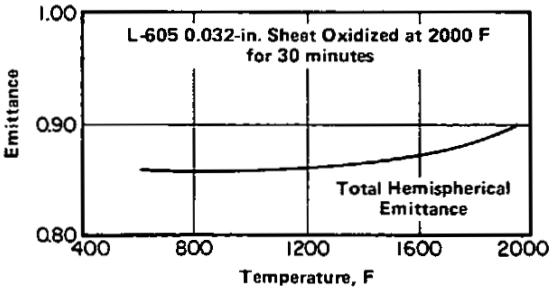

FIGURE 2.024. EMITTANCE (11)

L-605			
Medium	Concentration, weight percent	Temperature	Corrosion Rate, mils/year
Acetic Acid	10	Boiling	0.1
	99	Boiling	Nil
Hydrochloric Acid	10	Room	0.2
	5	Boiling	>1000
	10	Boiling	>1000
Nitric Acid	10	Boiling	0.8
	65	Boiling	53
Phosphoric Acid	10	Boiling	2
	55	Boiling	4
	85	Boiling	144
Sulfuric Acid	10 (vol)	Boiling	140
	96 (vol)	Boiling	76
Sulfuric Acid Plus Ferric Sulfate	50 (vol) + 4.2	Boiling	26

TABLE 2.0311. CORROSION RATES IN SEVERE AQUEOUS MEDIA (81)

Co
20 Cr
15 W
10 Ni

L-605

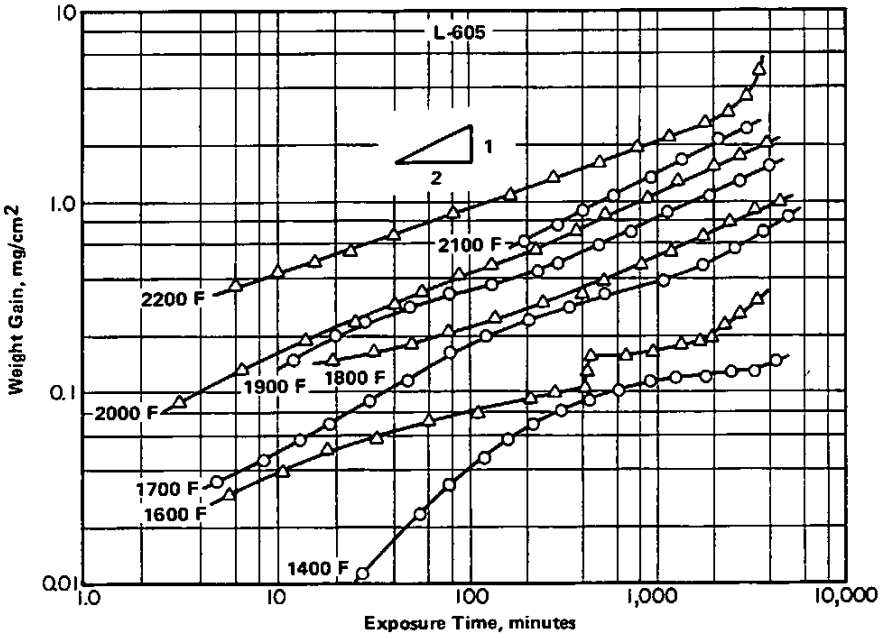

FIGURE 2.0322. OXIDATION WEIGHT GAIN AS A FUNCTION OF TIME FOR L-605 IN STILL AIR AT 1400 TO 2200 F (68)

Co
20 Cr
15 W
10 Ni
L-605

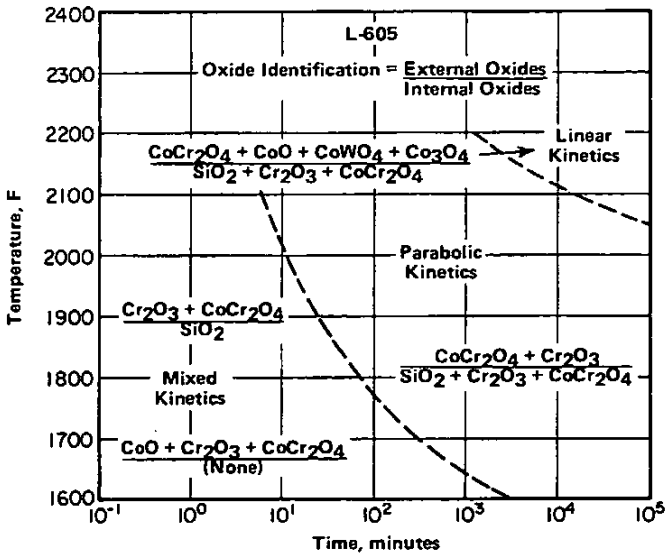

FIGURE 2.0323. SCHEMATIC SUMMARY OF L-605 OXIDATION PROCESS (82)

L-605					
Exposure Conditions		Zone Thickness, mils/side			
Temperature, F	Time, hours[a]	Surface Scale	Intergranular Penetration	Alloy Depletion	Total[b]
1560	500	0.2	0.3	0.3	0.5
1740	500	0.4	0.8	1.5	1.9
1830	500	1.0	1.0	2.2	3.2
	1,000	0.7	3.6	3.6	4.3
	5,000	2.0	4.0	4.0	6.0
	10,000	2.0 (2.0)[c]	4.0	4.0	8.0
2100	500	1.6	1.5	3.0	4.6
	3000	–	–	–	175

(a) 500-hour and 3000-hour test specimens were cylindrical, 0.25 to 0.5-inch diameter. Remaining test specimens were sheet, 0.06 to 0.08 inch thick.
(b) Total is surface scale plus greater of either intergranular penetration or alloy depletion.
(c) Number in parentheses is thickness of scale that spalled.

TABLE 2.0324. LONG-TIME OXIDATION IN STILL AIR (83)

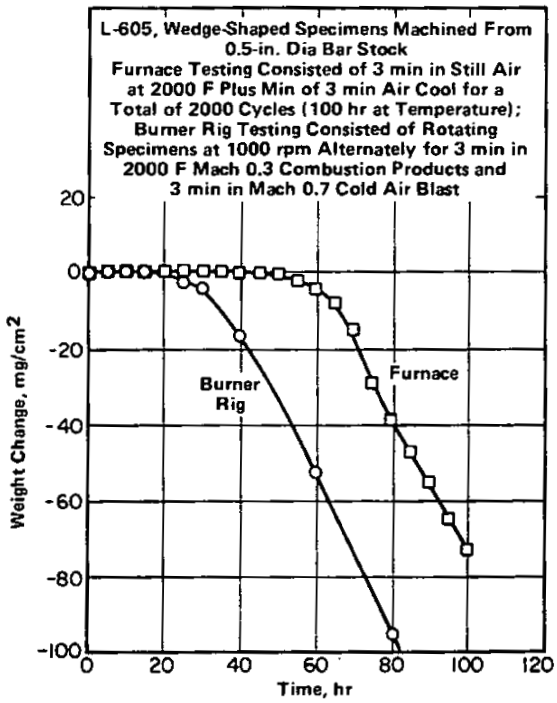

FIGURE 2.0325. OXIDATION WEIGHT CHANGES DURING CYCLIC FURNACE AND BURNER RIG EXPOSURES AT 2000 F FOR L-605 (84)

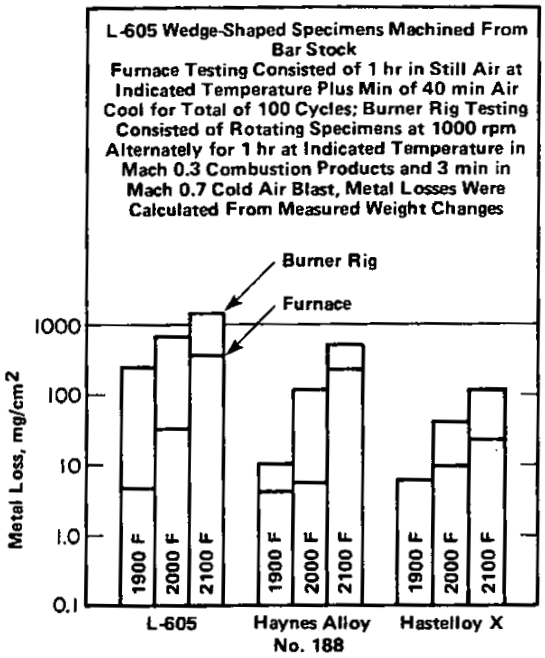

Co
20 Cr
15 W
10 Ni
L-605

FIGURE 2.0326. CALCULATED METAL LOSSES AFTER CYCLIC FURNACE AND BURNER RIG OXIDATION EXPOSURES AT 1900 TO 2100 F FOR L-605, HAYNES ALLOY NO. 188, AND HASTELLOY X (84)

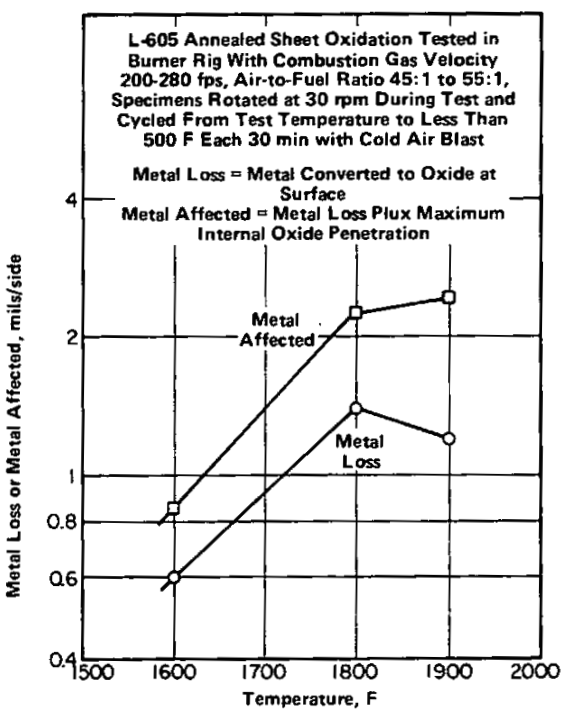

FIGURE 2.0327. DYNAMIC OXIDATION OF L-605 AFTER 100 HOURS AT 1600 TO 1900 F (85)

Co
20 Cr
15 W
10 Ni
L-605

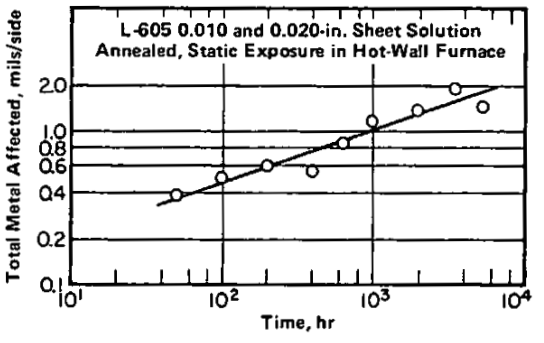

FIGURE 2.0328. OXIDATION BEHAVIOR AT 1800 F AND AIR PRESSURE OF 0.16 PSI (8 TORR) (86)

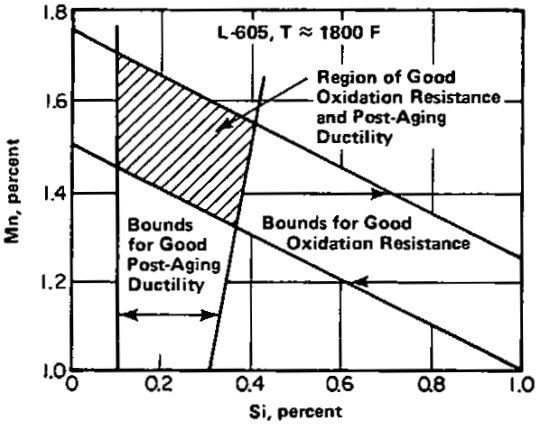

FIGURE 2.03210. EFFECT OF SILICON AND MANGANESE CONTENT ON OXIDATION RESISTANCE AND POST-AGING DUCTILITY (23)

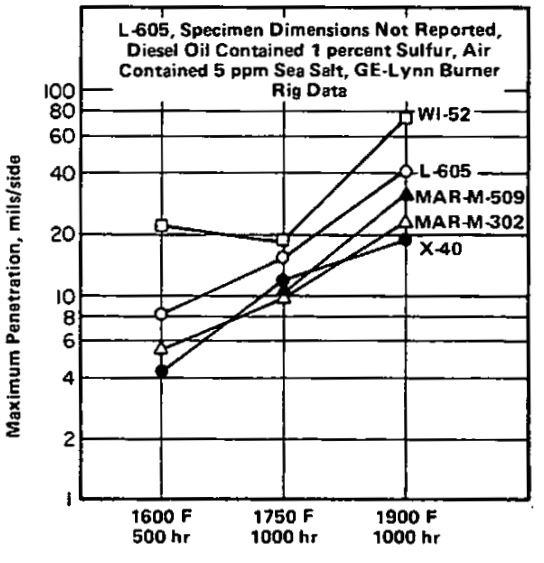

FIGURE 2.0332. DYNAMIC HOT CORROSION OF L-605 AND FOUR OTHER COBALT-BASE ALLOYS AT 1600 TO 1900 F (68)

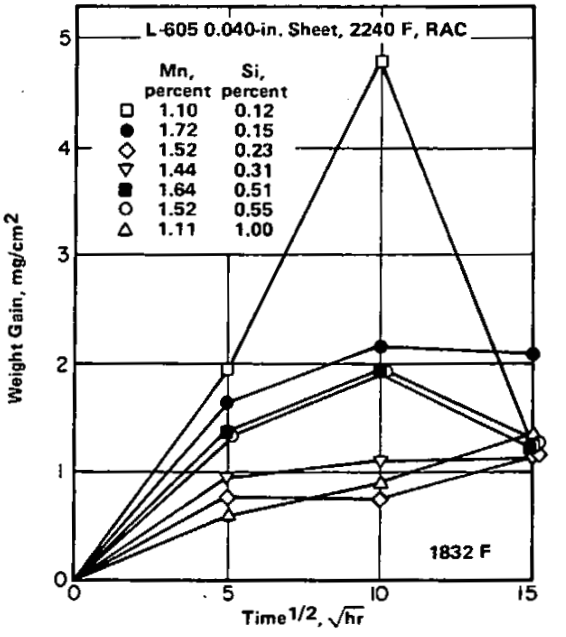

FIGURE 2.0329. EFFECT OF SILICON AND MANGANESE CONTENT ON OXIDATION OF SHEET IN AIR AT 1832 F (23)

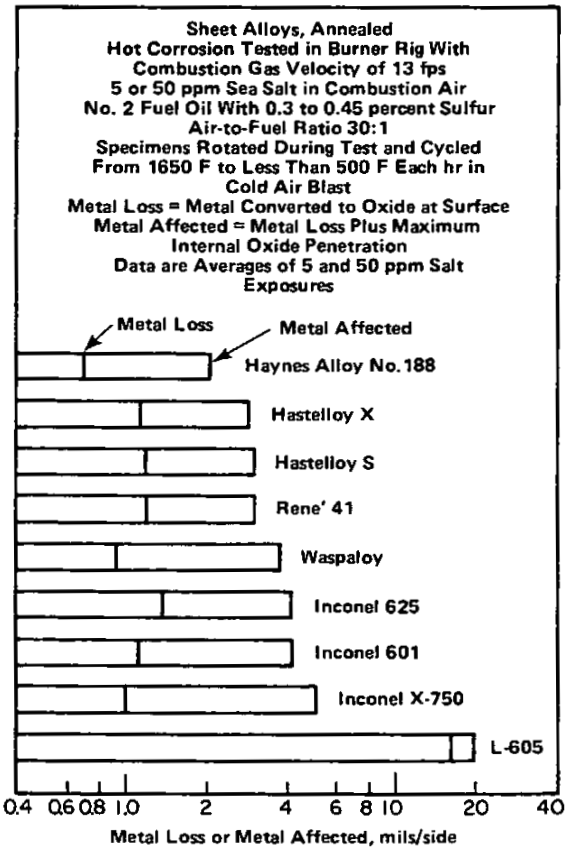

FIGURE 2.0333. DYNAMIC HOT CORROSION OF L-605 AND OTHER SHEET SUPERALLOYS AFTER 200 HOURS AT 1650 F (69)

Co
20 Cr
15 W
10 Ni

L-605

L-605[a]					
	Exposure Conditions		Post-Exposure		
Metallurgical Condition	Time, hours	Atmosphere	F_{tu}, ksi	Elongation, percent[f]	Hydrogen Content, ppm
CR[b]	100	Air	209	2	3.0
	100	Hydrogen	188	(c)	3.0
	1,000	Air	206	3	–
	1,000	Hydrogen	–	(c)	3.5
SA[d]	100	Air	86	12[e]	–
	100	Hydrogen	88	12[e]	2.5
	1,000	Air	99	3	–
	1,000	Hydrogen	84	3[e]	3.0

(a) 0.65 percent Si.
(b) Cold-rolled 25 percent.
(c) Broke in grip.
(d) Solution annealed 1 hour at 2250 F, AC.
(e) Numerous edge cracks during tensile testing.
(f) Gage section 1.2 by 0.37 by 0.025 inch.

TABLE 2.0342. EFFECT OF HYDROGEN EXPOSURE AT 1200 F ON ROOM TEMPERATURE STRENGTH AND DUCTILITY (70)

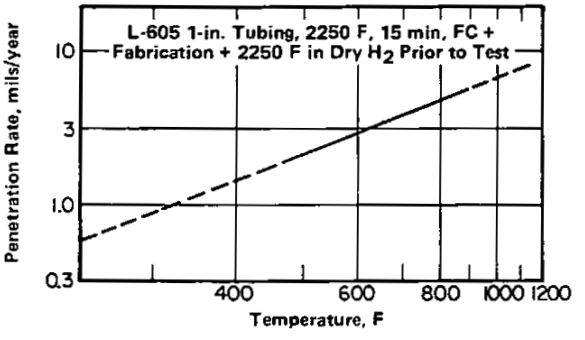

FIGURE 2.0362. MAXIMUM PENETRATION RATE OF MECURY IN THERMAL CONVECTION, TWO-PHASE LOOPS (48)

L-605						
Product Form	AMS Spec.	Thickness, inch	F_{ty}, ksi Min	F_{ty}, ksi Max	F_{tu}, ksi Min	Elongation, percent, Min[a]
Sheet	5537	≤0.020	55	80	130	30
		>0.020-0.032	55	80	130	35
		>0.032-0.043	55	80	130	40
		>0.043	55	80	130	45
Bars, Forgings, and Rings	5759	(Not specified)	45	–	125	30

(a) Elongation in 2 in. for sheet, 4D for bars, forgings, and rings.

Note: The original AMS documents should be consulted for complete specification details.

TABLE 3.011. SPECIFIED MECHANICAL PROPERTIES AT ROOM TEMPERATURE (1,2)

Co
20 Cr
15 W
10 Ni

L-605

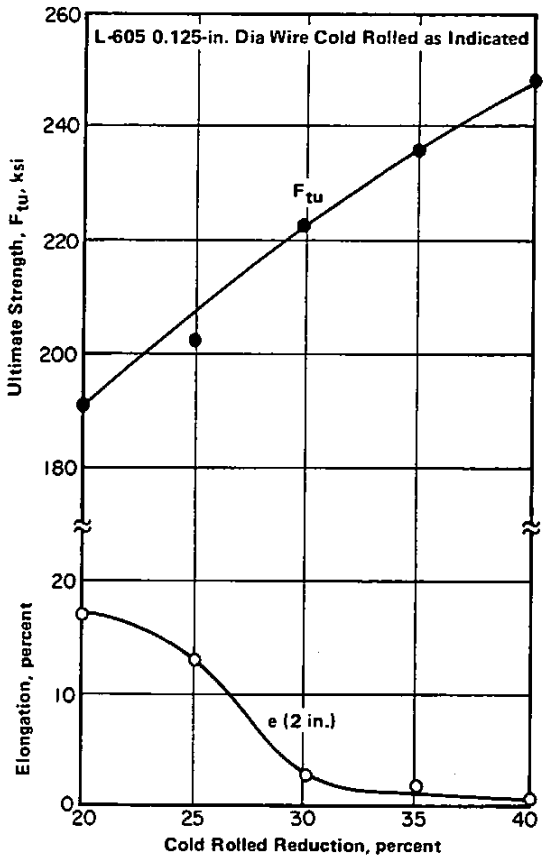

FIGURE 3.0211. EFFECT OF COLD REDUCTION ON TENSILE PROPERTIES OF 0.125-INCH WIRE (29,57)

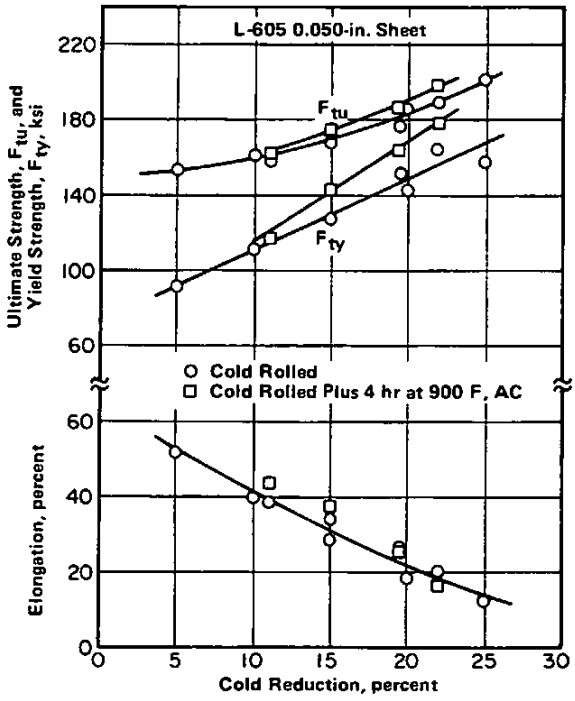

FIGURE 3.0212. EFFECTS OF COLD ROLLING AND COLD ROLLING PLUS 900 F AGING ON TENSILE PROPERTIES AT ROOM TEMPERATURE (62)

Co
20 Cr
15 W
10 Ni

L-605

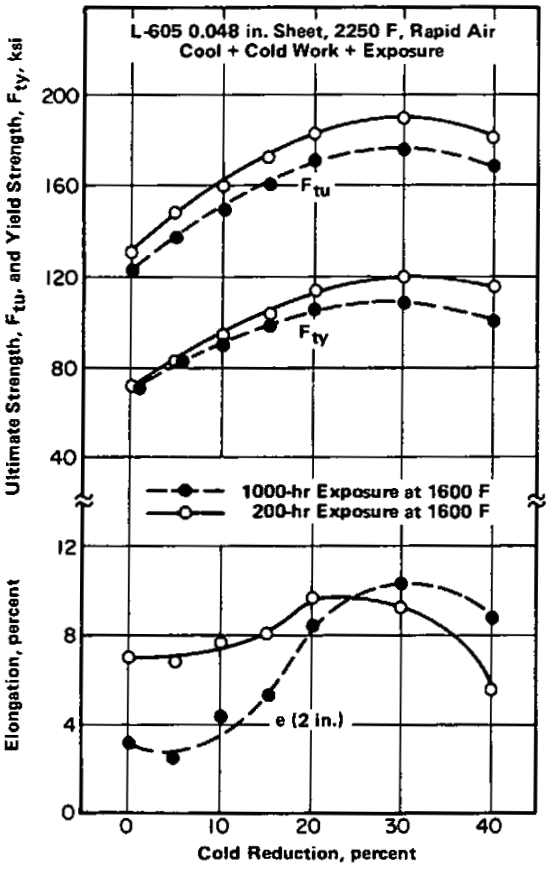

FIGURE 3.0214. EFFECT OF COLD REDUCTION ON TENSILE PROPERTIES AFTER PRIOR EXPOSURE TO 1600 F (51)

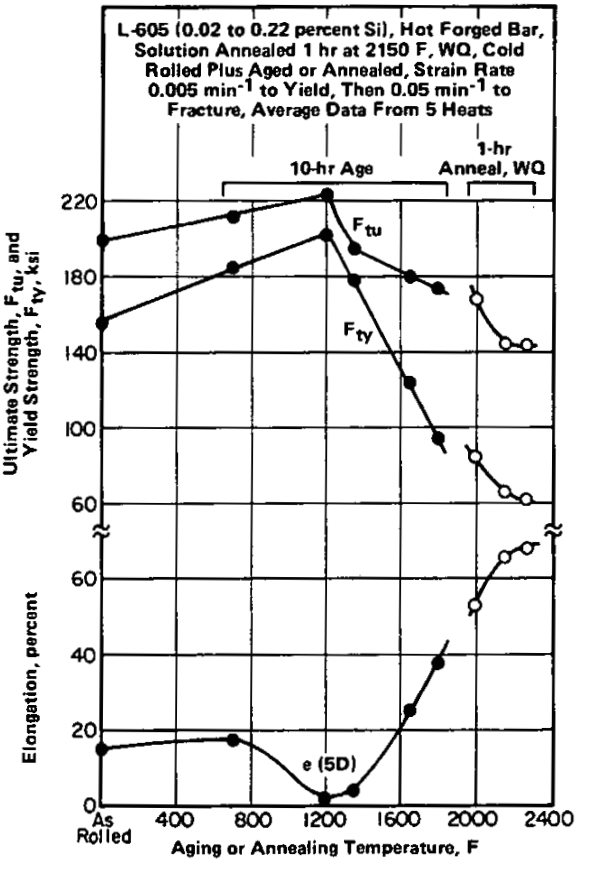

(a) Cold Rolled 25 percent

FIGURE 3.0215. EFFECTS OF AGING OR ANNEALING ON ROOM TEMPERATURE TENSILE PROPERTIES OF COLD ROLLED BAR (61)

Co
20 Cr
15 W
10 Ni

L-605

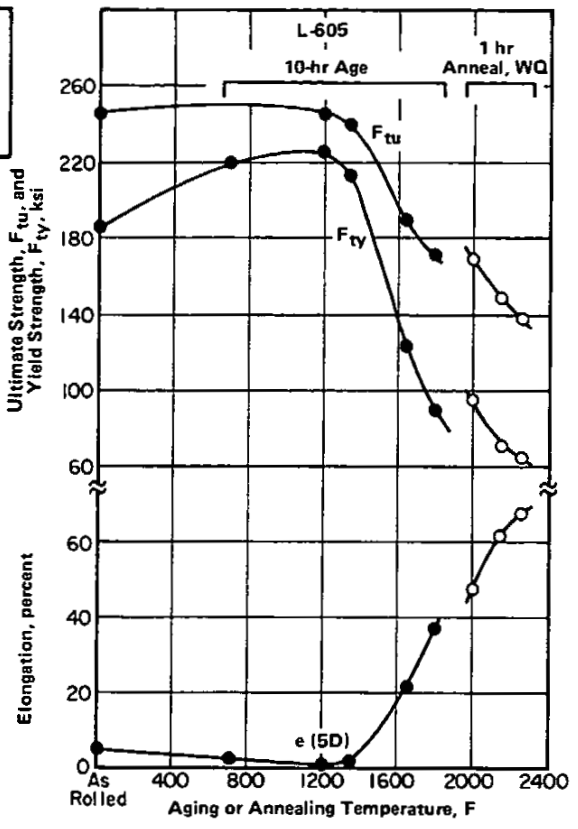

(b) Cold Rolled 40 percent

FIGURE 3.0215. (Continued)

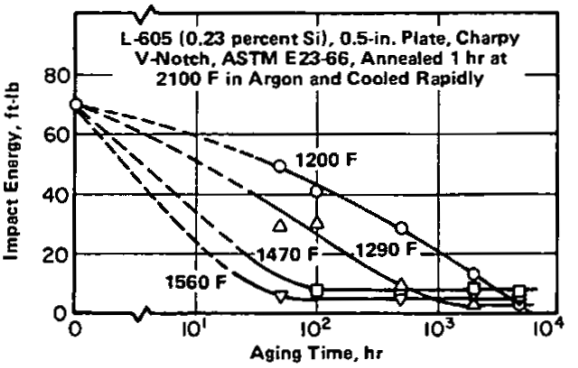

FIGURE 3.0231. EFFECTS OF AGING AT ELEVATED TEMPERATURES ON NOTCH-IMPACT ENERGY AT ROOM TEMPERATURE (87)

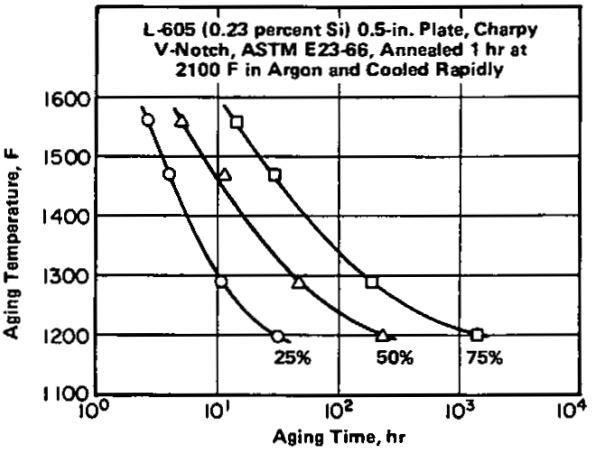

FIGURE 3.0232. AGING TIME-TEMPERATURE CURVES FOR 25, 50, AND 75 PERCENT REDUCTIONS IN NOTCH-IMPACT ENERGY AT ROOM TEMPERATURES (87)

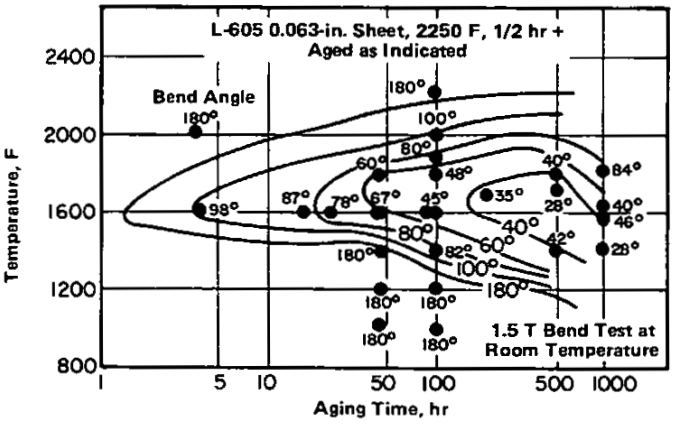

FIGURE 3.0241. EFFECT OF AGING TIME AND TEMPERATURE ON EMBRITTLEMENT OF SHEET AS DETERMINED BY A 1.5 T BEND TEST (46)

Co
20 Cr
15 W
10 Ni
L-605

L-605						
Processing				Tensile Strength[d]		
Initial Cold Reduction,[a] percent	Intermediate Solution Anneal, hours/F[b]	Secondary Cold Reduction, percent	Final Age, hours/F	F_{Ntu},[c] ksi	F_{tu}, ksi	Ratio, F_{Ntu}/F_{tu}
25	–	–	–	326.8	185.9	1.76
25	1/2250	25	–	294.6	214.4	1.37
25	1/2150	25	–	299.2	223.5	1.32
25	1/2150	25	10/700	324.4	244.3	1.33
25	1/2150	25	1/1200	240.1	247.7	0.97
40	–	–	–	306.5	258.5	1.19
40	1/2250	40	–	253.4	251.4	1.01
40	1/2150	40	–	236.6	255.3	0.93
40	1/2150	40	10/700	267.4	249.1	1.07
40	1/2150	40	1/1200	166.7	296.7	0.56

(a) Starting material was hot forged bar stock, solution annealed 1 hour at 2150 F, WQ.
(b) Plus WQ.
(c) K_t = 7-8, specimen gage length 0.19-inch diameter by 1.0 inch long.
(d) Average of duplicate tests from several heats.

TABLE 3.02711. NOTCHED TENSILE STRENGTH OF COLD WORKED AND COLD WORKED PLUS AGED BAR AT ROOM TEMPERATURE (61)

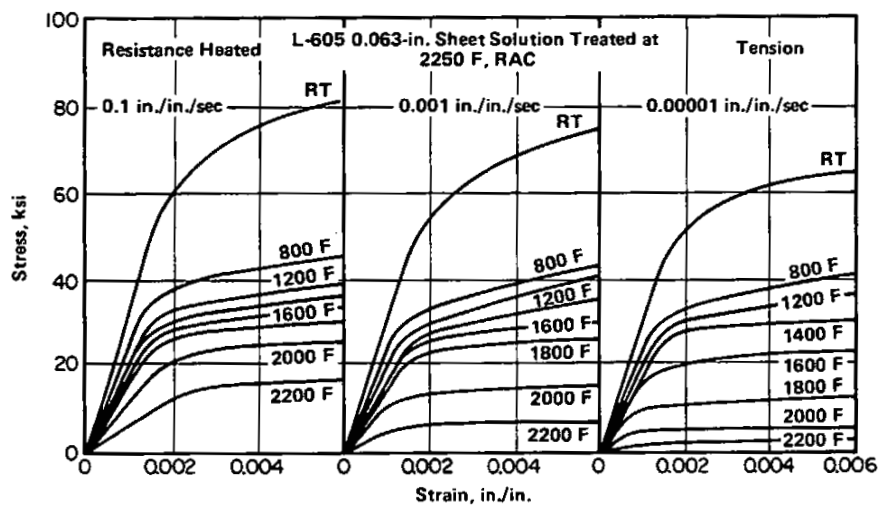

FIGURE 3.0312. STRESS-STRAIN CURVES IN TENSION FOR 0.063-INCH SHEET AT ROOM AND ELEVATED TEMPERATURES AT SEVERAL STRAIN RATES (30)

Co
20 Cr
15 W
10 Ni

L-605

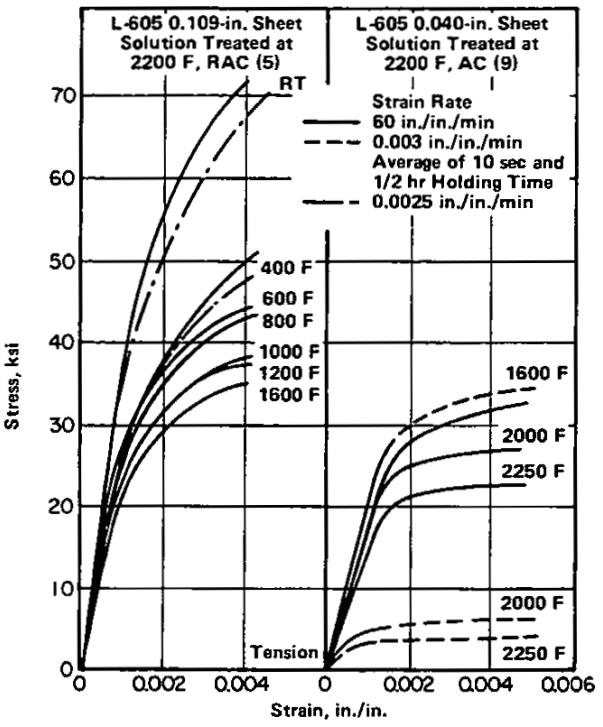

FIGURE 3.0313. STRESS-STRAIN CURVES FOR 0.109 AND 0.040-INCH SHEET AT ROOM AND ELEVATED TEMPERATURES AT SEVERAL STRAIN RATES (5,9)

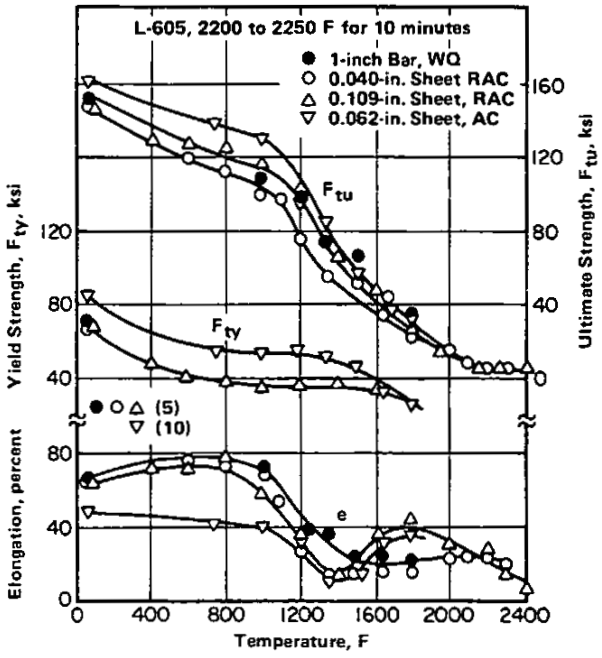

FIGURE 3.0314. EFFECT OF TEST TEMPERATURE ON TENSILE PROPERTIES OF BAR AND SHEET (5,10)

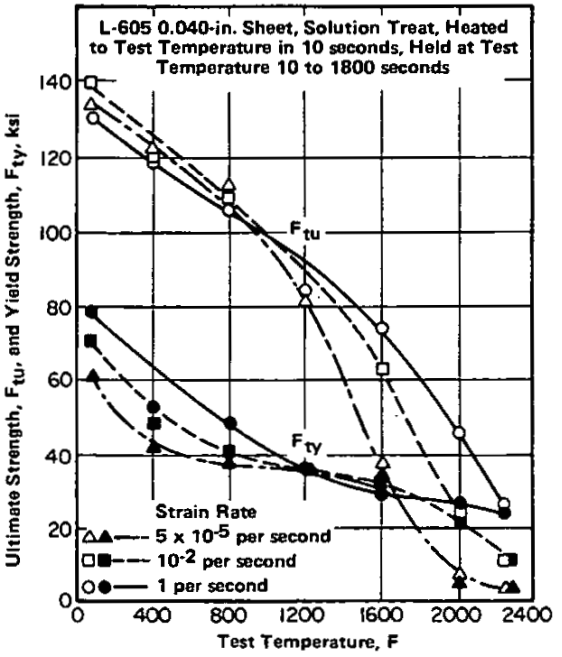

FIGURE 3.0315. EFFECT OF TEST TEMPERATURE AND STRAIN RATE ON TENSILE AND YIELD STRENGTH OF SHEET (39,40,41,57)

Co
20 Cr
15 W
10 Ni
L-605

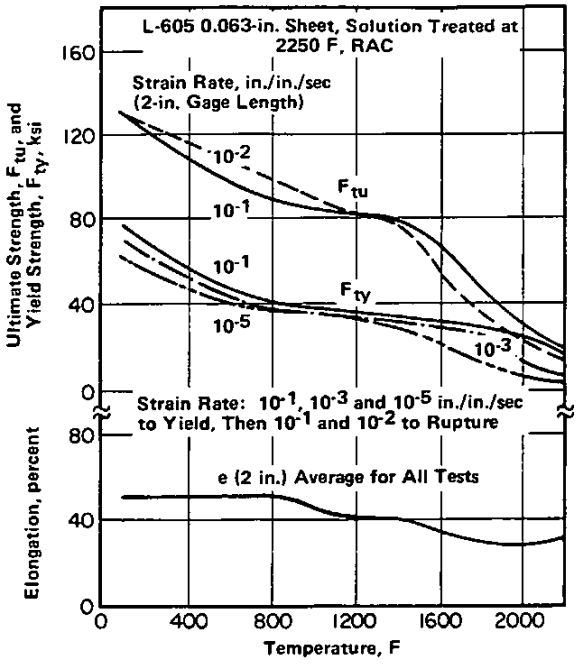

FIGURE 3.0316. TYPICAL EFFECTS OF TEST TEMPERATURE AND STRAIN RATE ON TENSILE PROPERTIES OF SHEET (30)

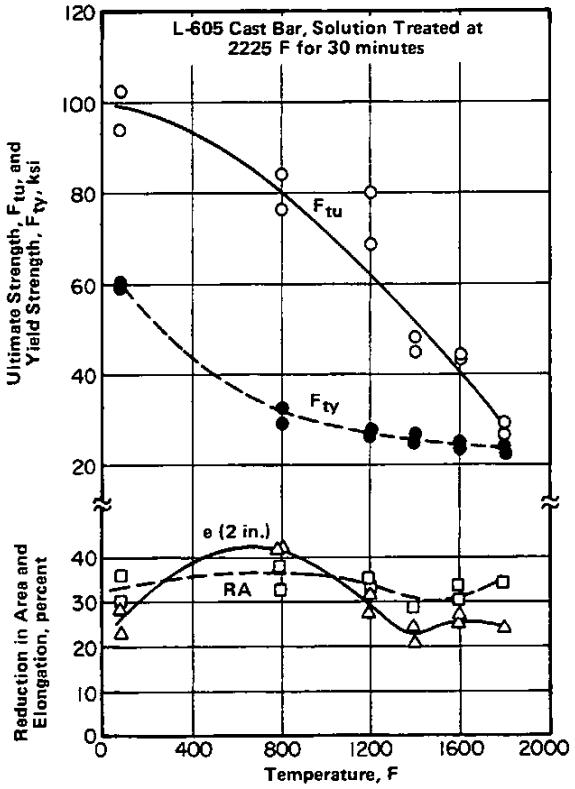

FIGURE 3.0317. EFFECT OF TEST TEMPERATURE ON TENSILE PROPERTIES OF CAST BAR IN SOLUTION TREATED CONDITION (27)

Co
20 Cr
15 W
10 Ni

L-605

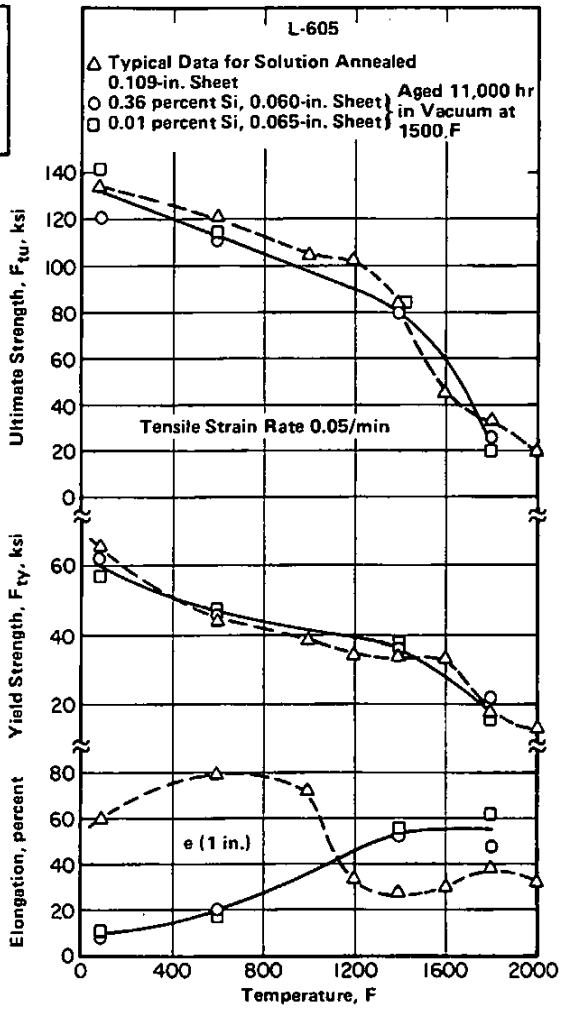

FIGURE 3.0318. EFFECT OF TEST TEMPERATURE ON TENSILE PROPERTIES OF SHEET AFTER 11,000-HOUR EXPOSURE AT 1500 F (88)

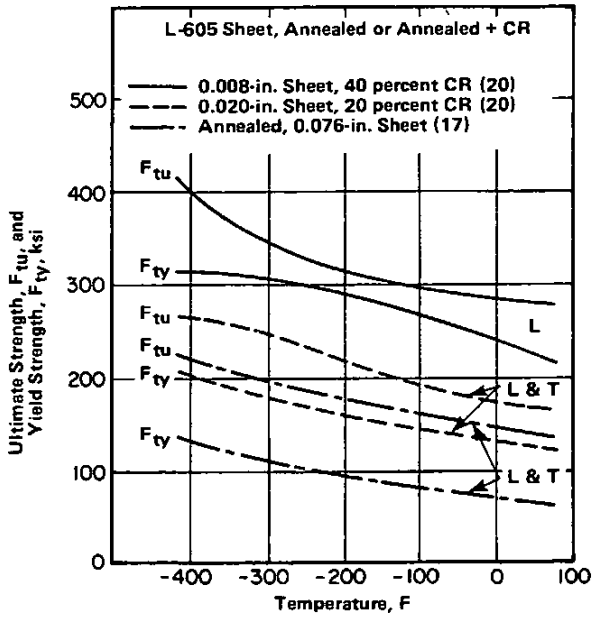

FIGURE 3.0319. EFFECT OF LOW TEST TEMPERATURE ON TENSILE AND YIELD STRENGTH OF SHEET (17,20)

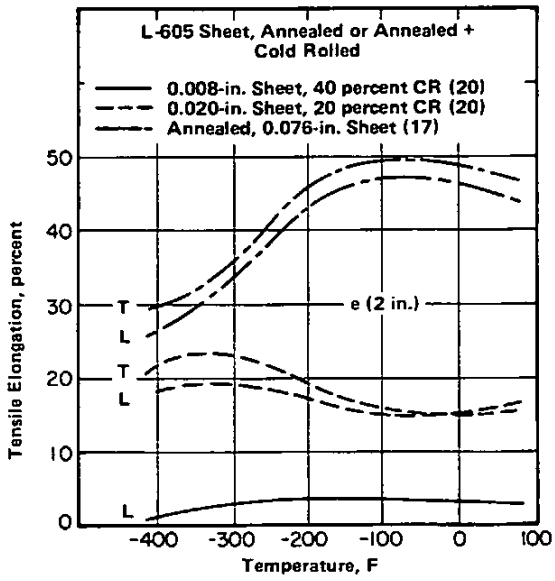

FIGURE 3.03110. EFFECT OF LOW TEST TEMPERATURE ON TENSILE ELONGATION OF SHEET (17)

Co
20 Cr
15 W
10 Ni

L-605

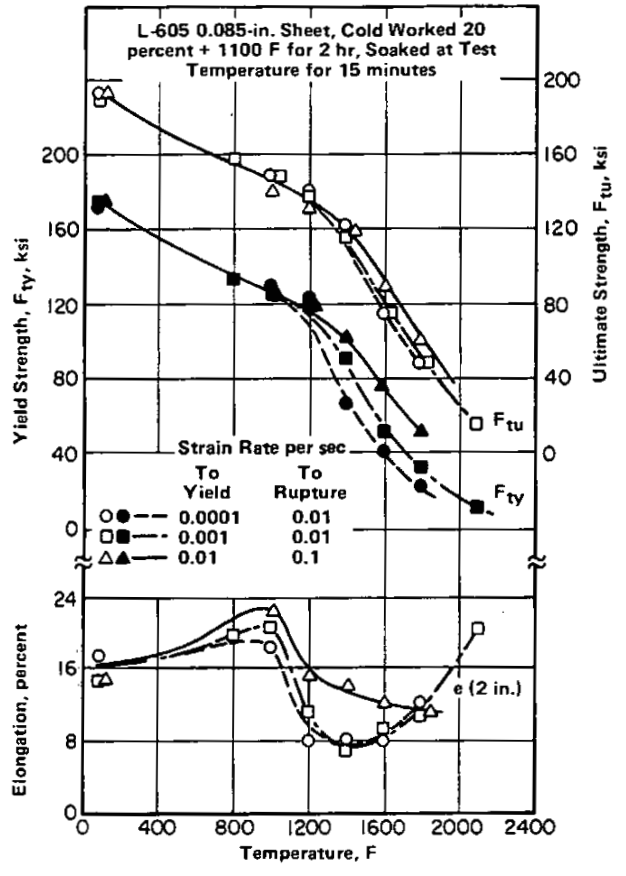

FIGURE 3.03111. EFFECT OF TEST TEMPERATURE AND STRAIN RATE ON TENSILE PROPERTIES OF 20 PERCENT COLD-WORKED SHEET (38,57)

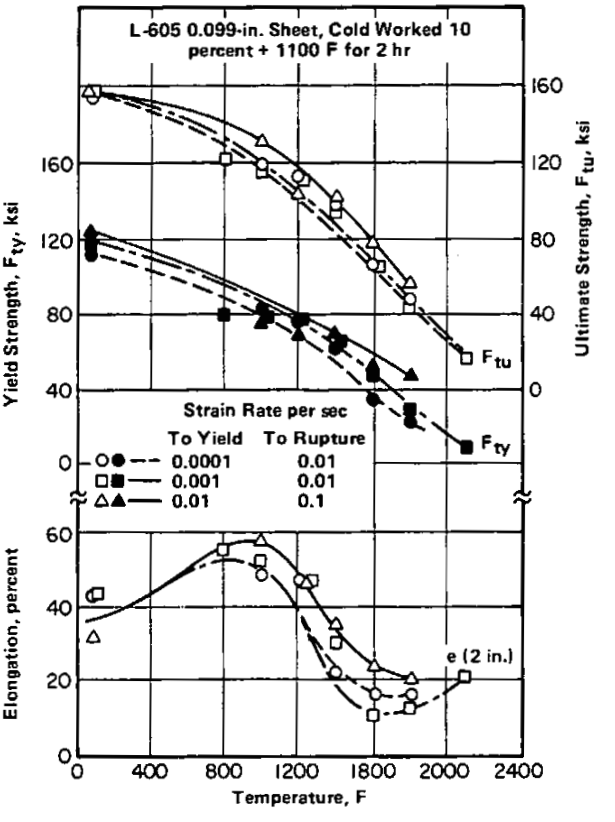

FIGURE 3.03112. EFFECT OF TEST TEMPERATURE AND STRAIN RATE ON TENSILE PROPERTIES OF 10 PERCENT COLD-WORKED AND AGED SHEET (38,57)

Co
20 Cr
15 W
10 Ni

L-605

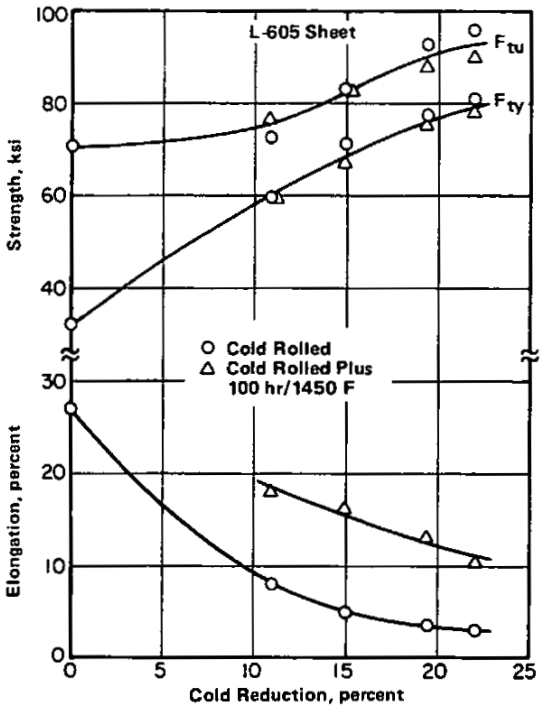

FIGURE 3.03113. EFFECTS OF COLD ROLLING AND COLD ROLLING PLUS 1450 F AGING ON TENSILE PROPERTIES AT 1450 F (62)

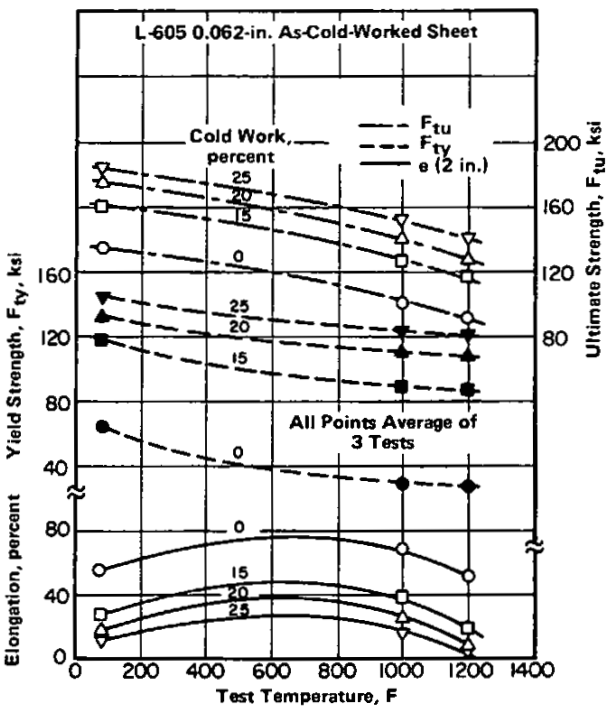

FIGURE 3.03114. EFFECT OF TEST TEMPERATURE ON TENSILE PROPERTIES OF AS-COLD-WORKED SHEET (27)

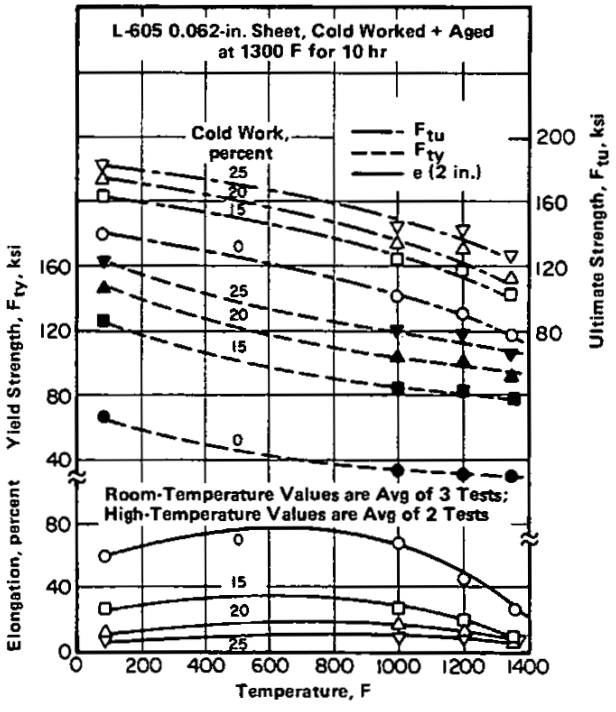

FIGURE 3.03115. EFFECT OF TEST TEMPERATURE ON TENSILE PROPERTIES OF COLD-WORKED AND AGED SHEET (27)

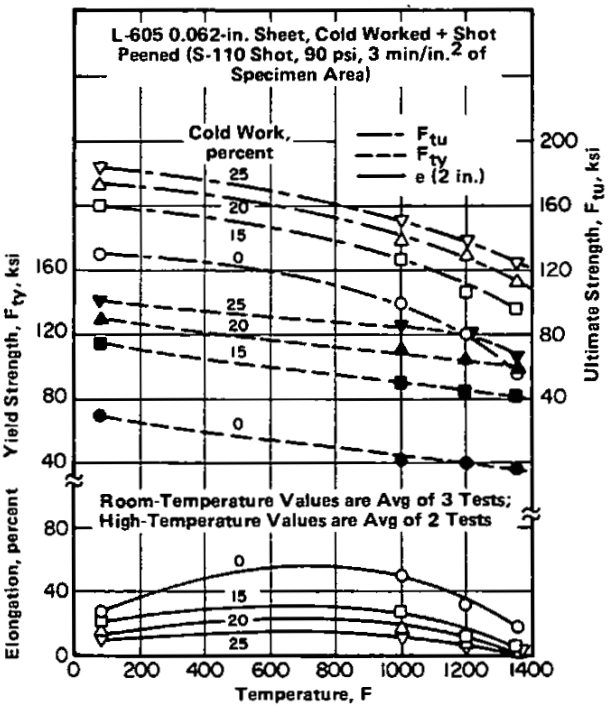

FIGURE 3.03116. EFFECT OF TEST TEMPERATURE ON TENSILE PROPERTIES OF COLD-WORKED AND SHOT-PEENED SHEET (27)

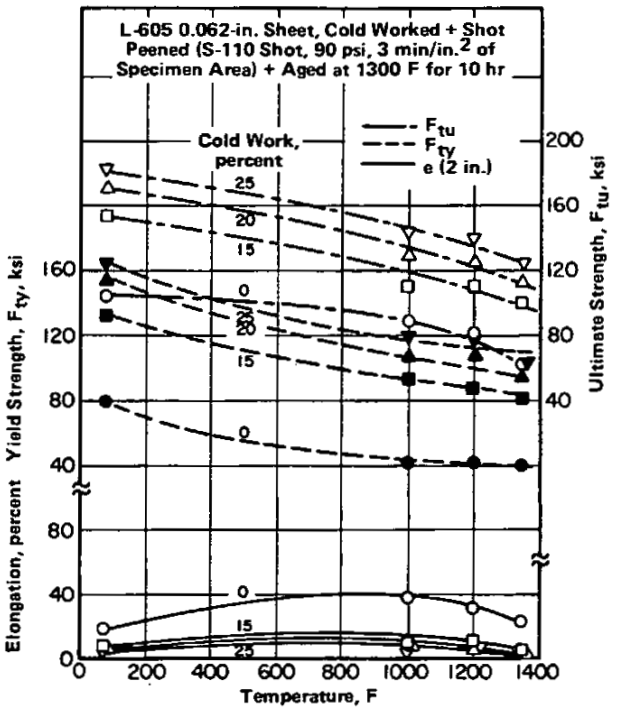

FIGURE 3.03117. EFFECT OF TEST TEMPERATURE ON TENSILE PROPERTIES OF COLD-WORKED, SHOT-PEENED, AND AGED SHEET (27)

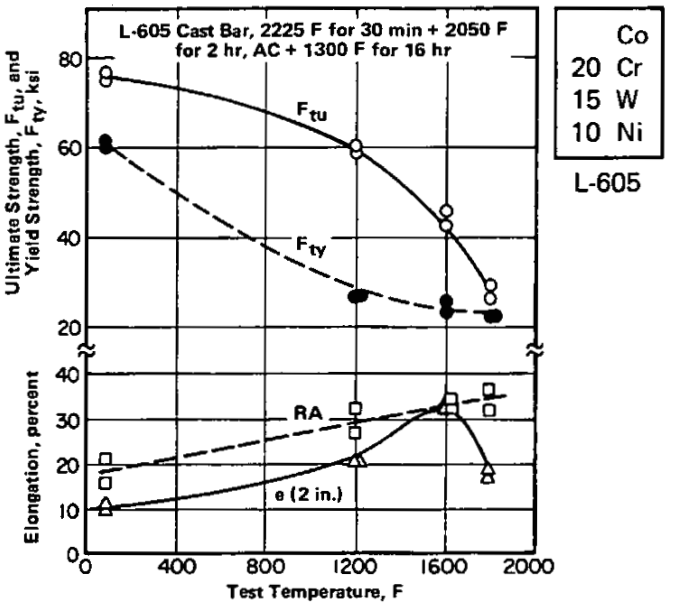

FIGURE 3.03118. EFFECT OF TEST TEMPERATURE ON TENSILE PROPERTIES OF CAST BAR WHEN SOLUTION TREATED, STRESS RELIEVED, AND AGED (27)

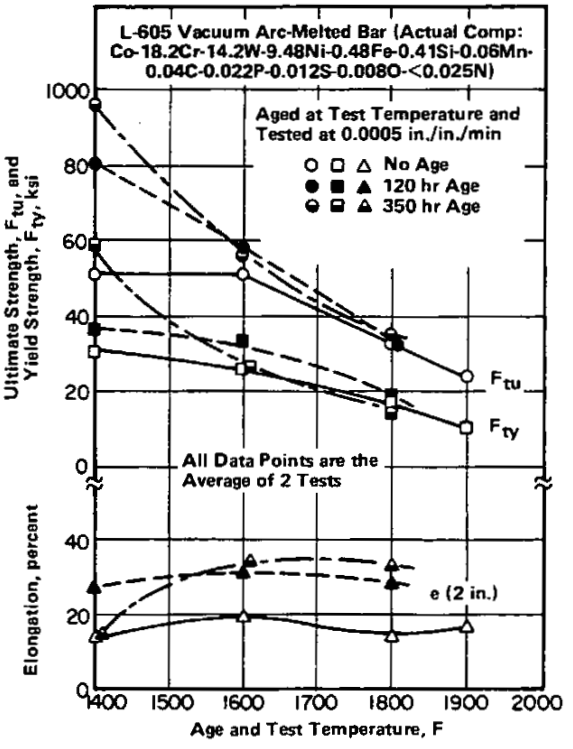

FIGURE 3.03119. EFFECT OF AGING TIME AND TEMPERATURE ON ELEVATED TEMPERATURE TENSILE PROPERTIES OF VACUUM ARC-MELTED BAR (35,37)

Co
20 Cr
15 W
10 Ni

L-605

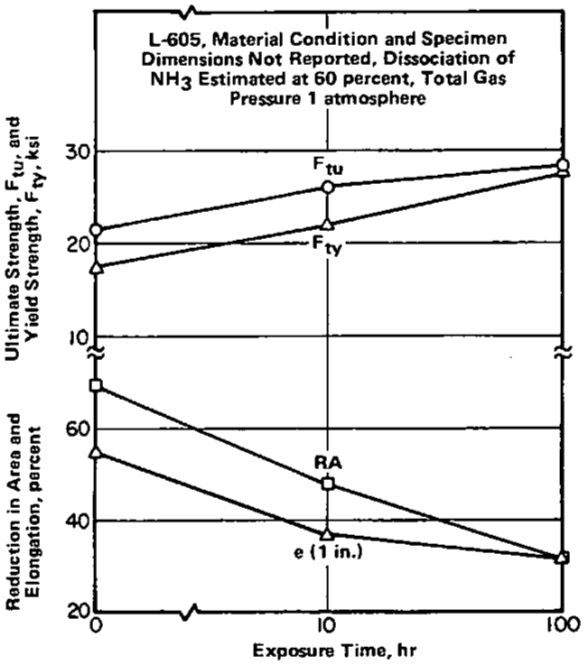

FIGURE 3.03120. TENSILE PROPERTIES OF L-605 AT 1800 F AFTER EXPOSURE TO PARTIALLY DISSOCIATED AMMONIA AT 1800 F (72)

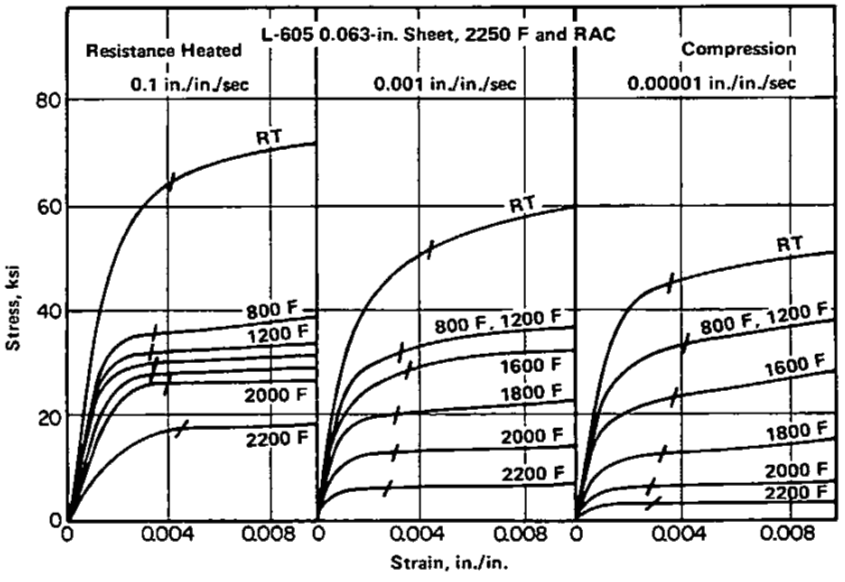

FIGURE 3.0321. STRESS-STRAIN CURVES IN COMPRESSION FOR SHEET AT ROOM AND ELEVATED TEMPERATURES AT SEVERAL STRAIN RATES (30)

Co
20 Cr
15 W
10 Ni

L-605

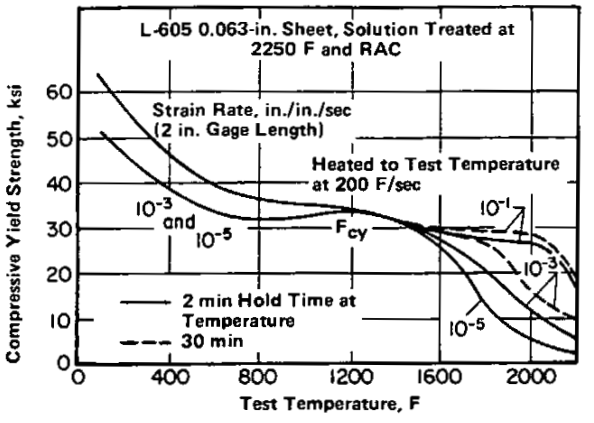

FIGURE 3.0322. TYPICAL EFFECT OF TEST TEMPERATURE AND STRAIN RATE ON COMPRESSIVE YIELD STRENGTH (30)

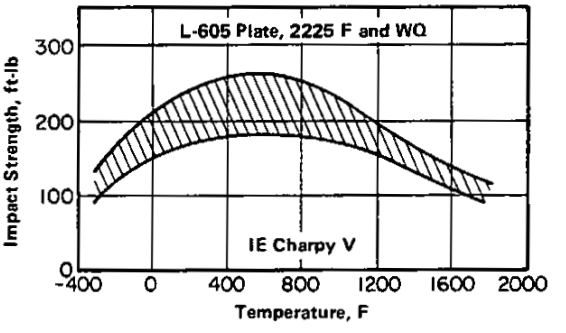

FIGURE 3.0331. EFFECT OF TEST TEMPERATURE ON IMPACT STRENGTH OF PLATE (5)

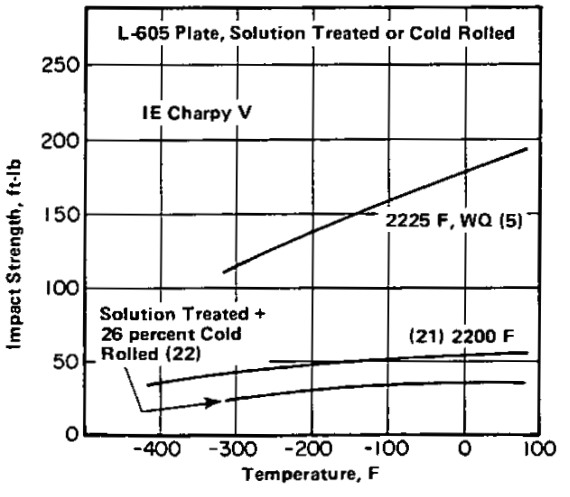

FIGURE 3.0332. EFFECT OF LOW TEST TEMPERATURE ON IMPACT STRENGTH OF SOLUTION TREATED OR SOLUTION TREATED AND COLD ROLLED PLATE (5,17,21,22)

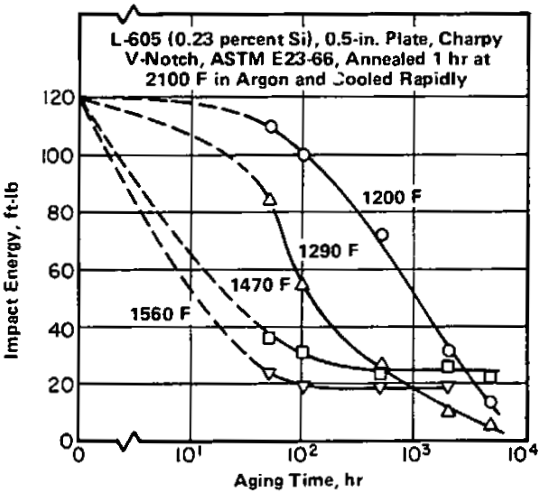

FIGURE 3.0333. EFFECTS OF AGING AT ELEVATED TEMPERATURES ON NOTCH-IMPACT ENERGY AT 570 F (87)

Co
20 Cr
15 W
10 Ni

L-605

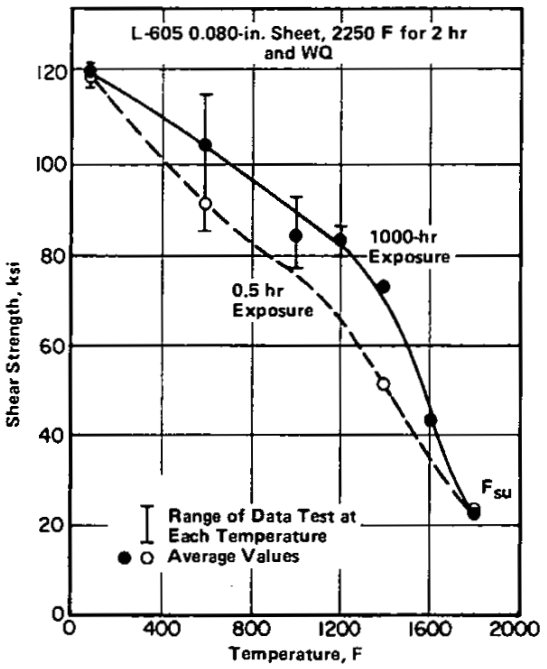

FIGURE 3.0351. EFFECT OF TEST TEMPERATURE ON SHEAR STRENGTH OF SHEET (47)

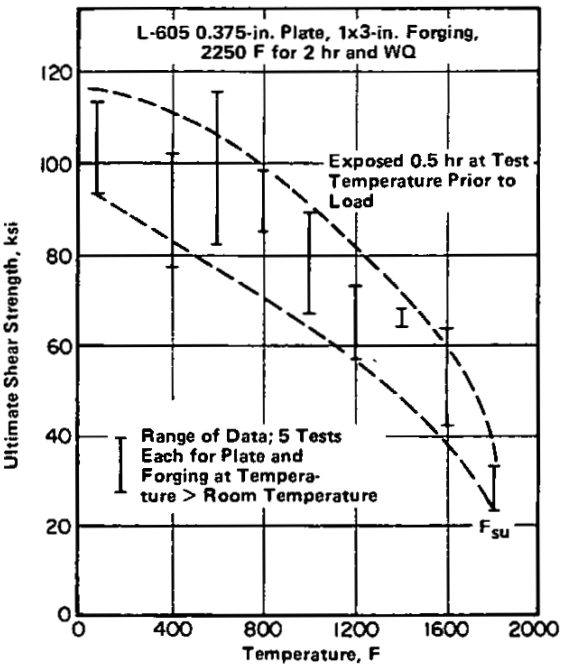

FIGURE 3.0352. EFFECT OF TEST TEMPERATURE ON SHEAR STRENGTH OF PLATE AND FORGING (47)

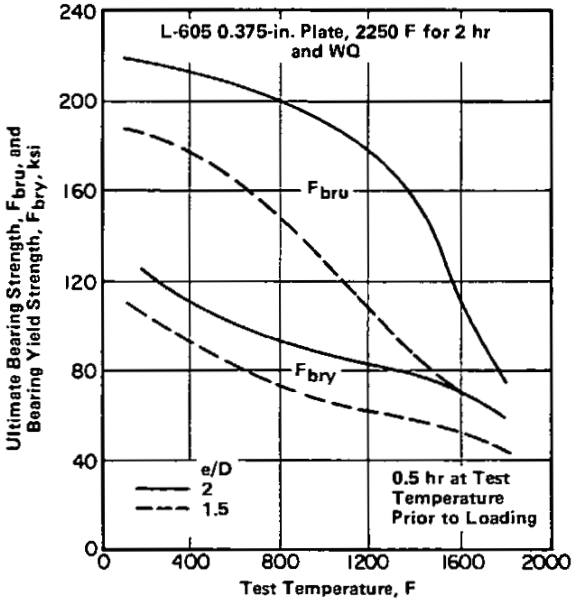

FIGURE 3.0361. EFFECT OF TEST TEMPERATURE ON BEARING ULTIMATE AND YIELD STRENGTH (47)

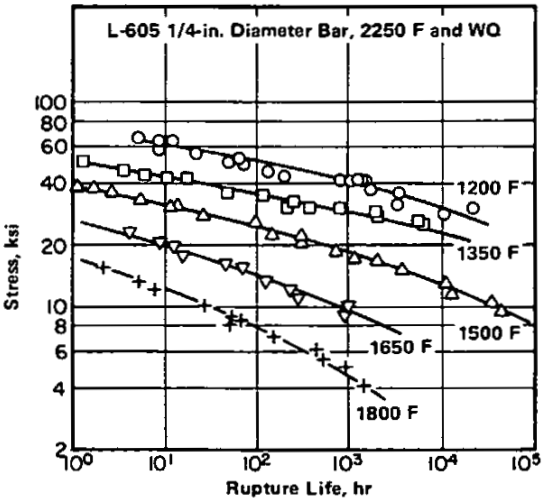

FIGURE 3.041. CREEP-RUPTURE CURVES FOR BAR AT TEMPERATURES FROM 1200 TO 1800 F FOR TIMES UP TO 40,000 HOURS (49,50)

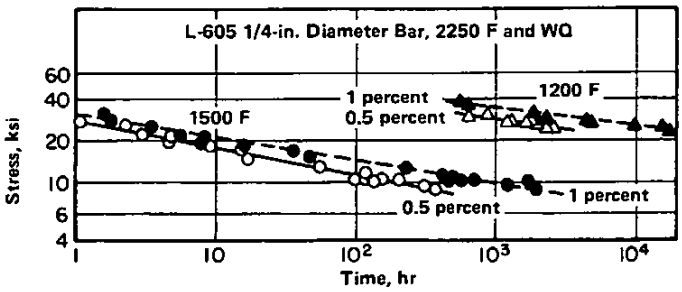

Co
20 Cr
15 W
10 Ni
L-605

FIGURE 3.042. STRESS REQUIRED TO PRODUCE TOTAL PLASTIC STRAINS OF 0.5 AND 1.0 PERCENT AT 1200 AND 1500 F (49)

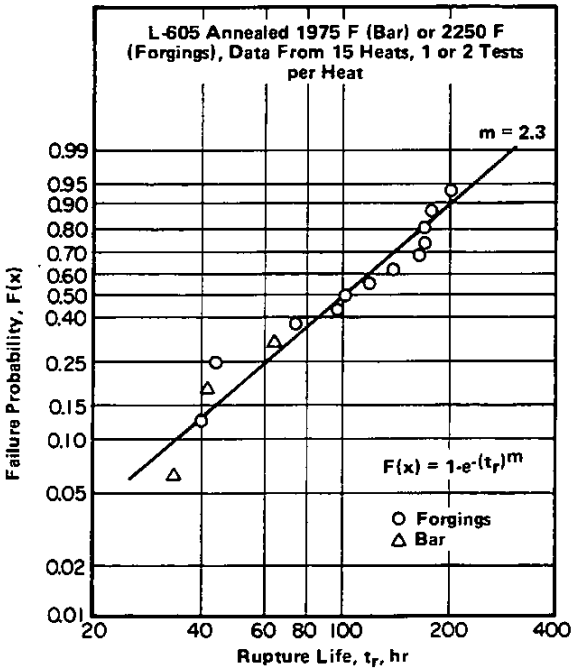

FIGURE 3.043. WEIBULL DISTRIBUTION OF CREEP-RUPTURE LIFE FOR BAR AND FORGINGS AT 1500 F AND 24 KSI (89)

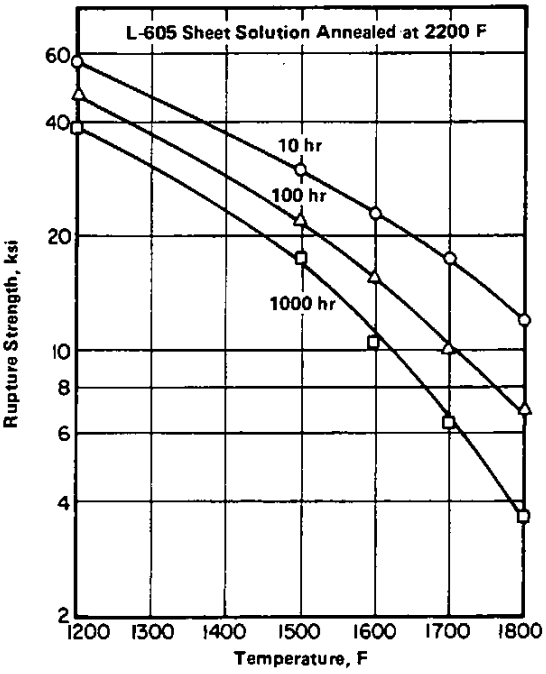

FIGURE 3.044. CREEP-RUPTURE STRENGTH AT ELEVATED TEMPERATURES (62)

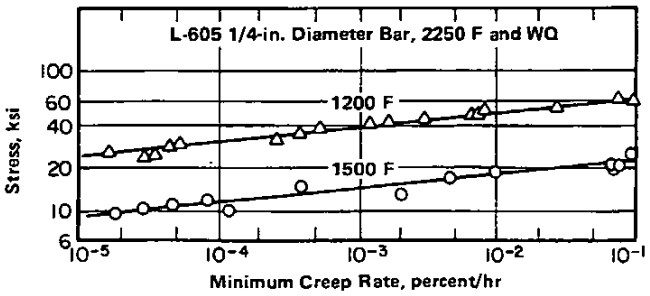

FIGURE 3.045. MINIMUM CREEP-RATE CURVES FOR BAR AT 1200 AND 1500 F (49)

Co
20 Cr
15 W
10 Ni

L-605

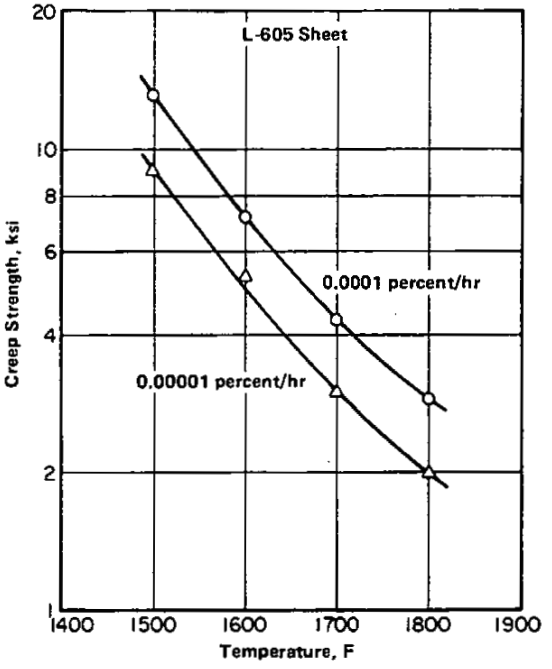

FIGURE 3.046. CREEP STRENGTH AT ELEVATED TEMPERATURES (62)

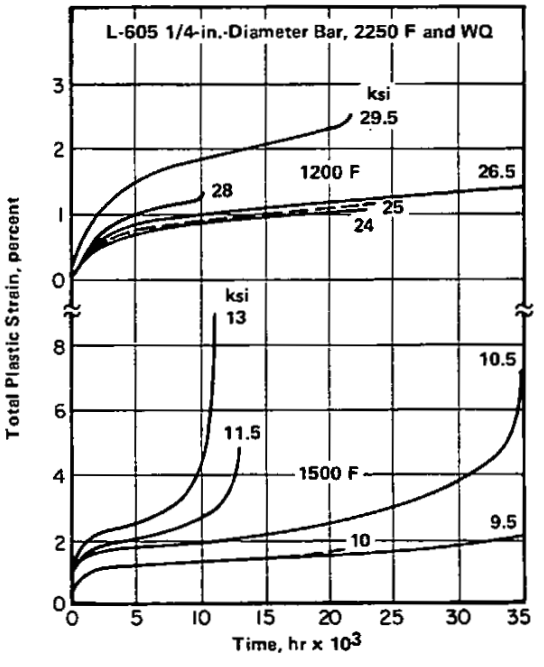

FIGURE 3.047. VERY LONG TIME CREEP CURVES FOR BAR AT 1200 AND 1500 F (49)

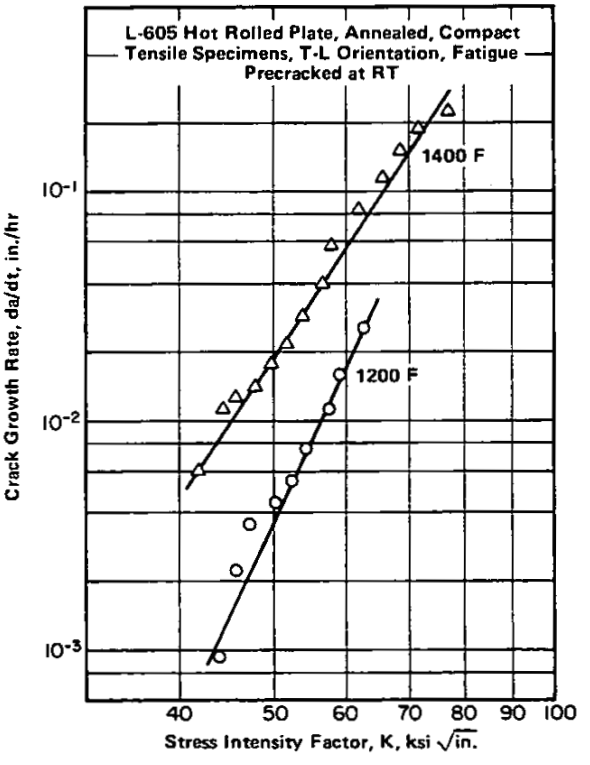

FIGURE 3.0410. CREEP CRACK GROWTH AT ELEVATED TEMPERATURES (77)

Co
20 Cr
15 W
10 Ni

L-605

L-605						
Condition	Test Temperature, F	Initial Stress, ksi	Residual Stress, ksi, After: 1 Hour	10 Hours	50 Hours	100 Hours
SA[a]	1050	70.0	–	–	–	42.0
	1200	45.0	–	–	–	19.4
	1350	25.0	–	–	–	14.0
HR[b]	1100	30.0	–	–	–	28.0
CW[c]	1400	80.3	32.5	23.7	13.9	–

(a) Hot-rolled 0.875-inch-dia bar, solution annealed at 2280 F and WQ.
(b) Hot-rolled 1.063-inch-dia bar.
(c) Solution annealed 30 min at 2225 F, WQ, cold extruded 30 percent and cold formed into bolt, 0.25-inch-dia by 1.562 inch long.

TABLE 3.0411. TORSIONAL STRESS RELAXATION AT ELEVATED TEMPERATURES (90)

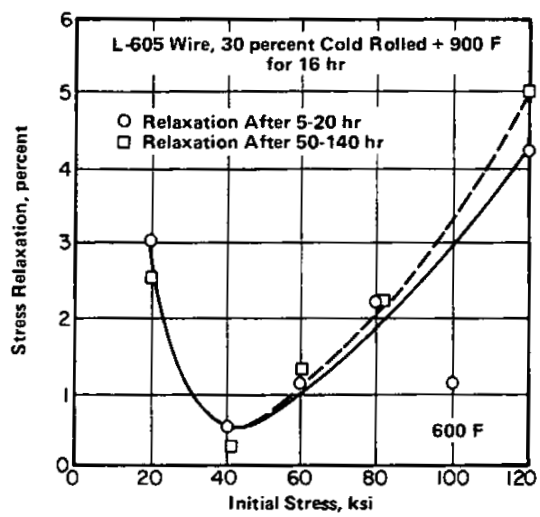

FIGURE 3.0412. STRESS RELAXATION OF WIRE AT 600 F (29)

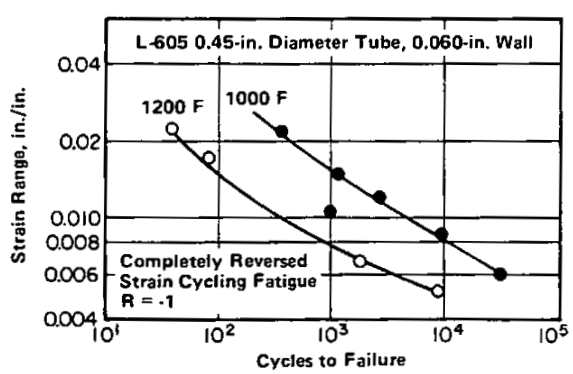

FIGURE 3.052. REVERSED STRAIN CYCLING FATIGUE OF HOLLOW TUBE AT 1000 AND 1200 F (56)

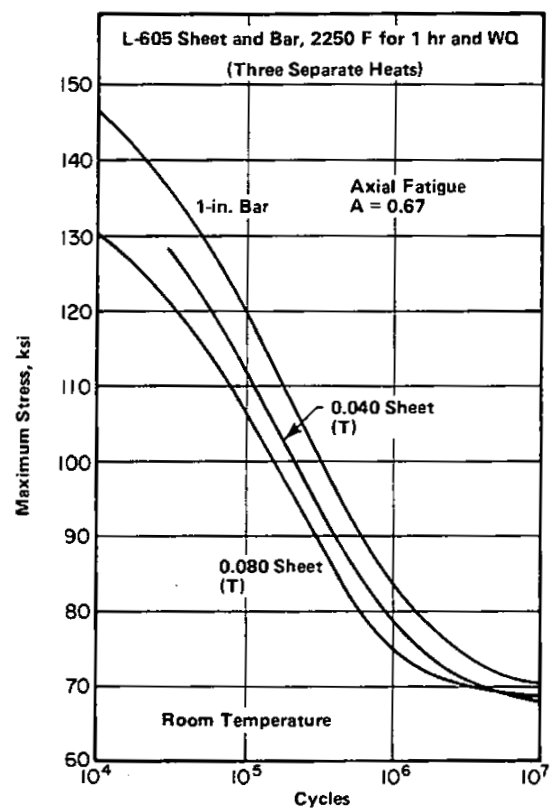

FIGURE 3.051. ROOM TEMPERATURE FATIGUE OF SHEET AND BAR IN AXIAL LOADING (47)

Co
20 Cr
15 W
10 Ni
L-605

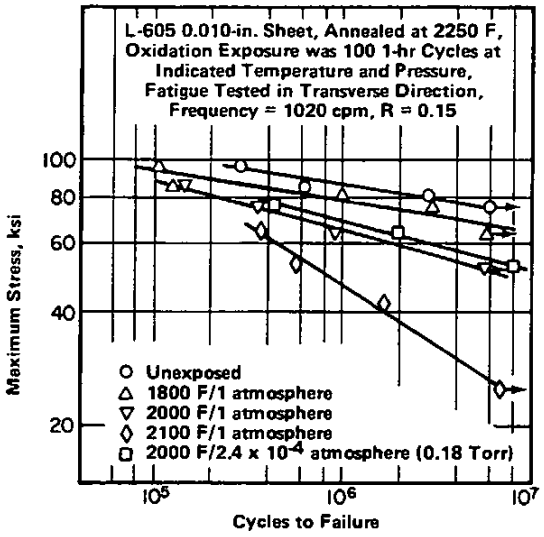

FIGURE 3.053. FATIGUE OF THIN SHEET AT ROOM TEMPERATURE AFTER 100-HOUR CYCLIC AIR EXPOSURES AT 1800 TO 2100 F (91)

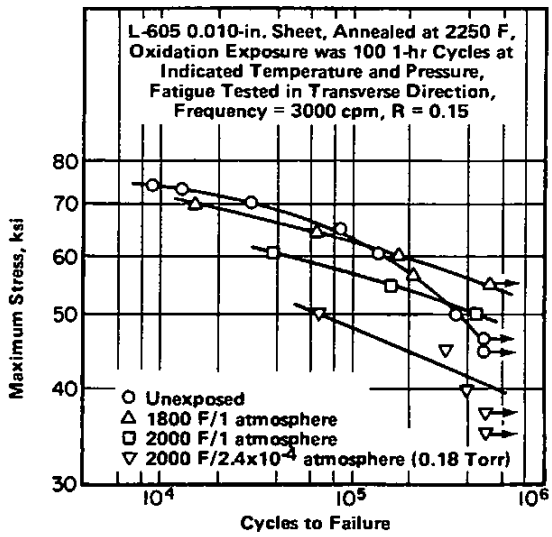

FIGURE 3.054. FATIGUE OF THIN SHEET AT 1400 F AFTER 100-HOUR CYCLIC AIR EXPOSURES AT 1800 AND 2000 F (91)

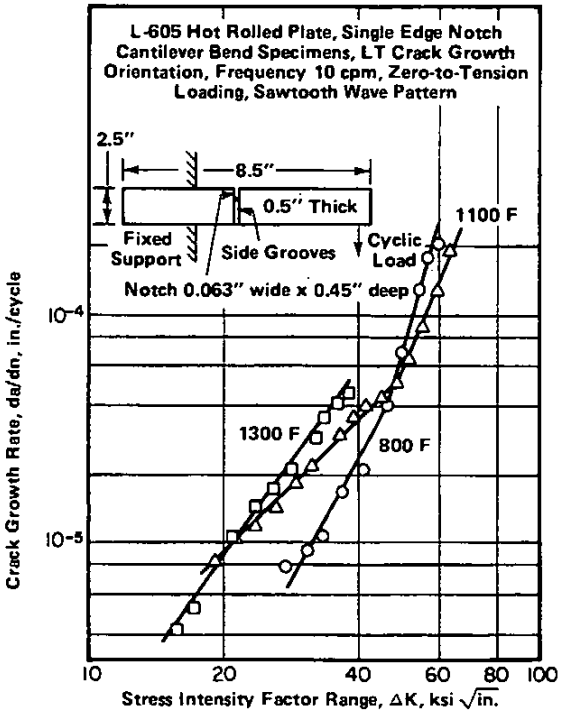

FIGURE 3.055. LOW CYCLE FATIGUE CRACK GROWTH AT ELEVATED TEMPERATURES (92)

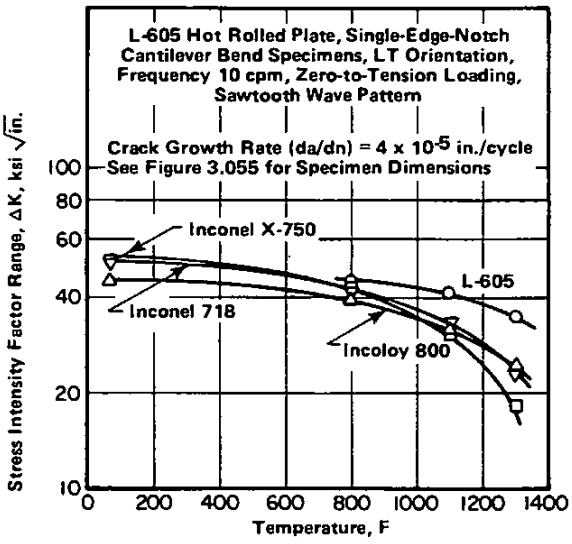

FIGURE 3.057. STRESS INTENSITY FACTOR RANGE AS A FUNCTION OF TEMPERATURE FOR FATIGUE CRACK GROWTH IN L-605 AND THREE OTHER HIGH-TEMPERATURE ALLOYS (92)

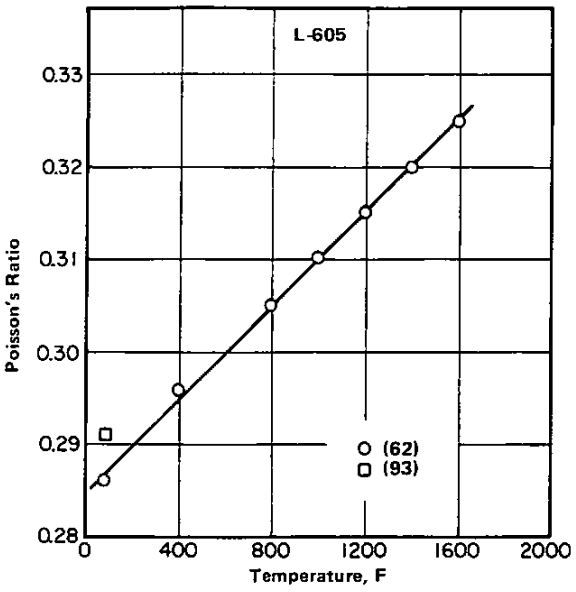

FIGURE 3.061. POISSON'S RATIO (62,93)

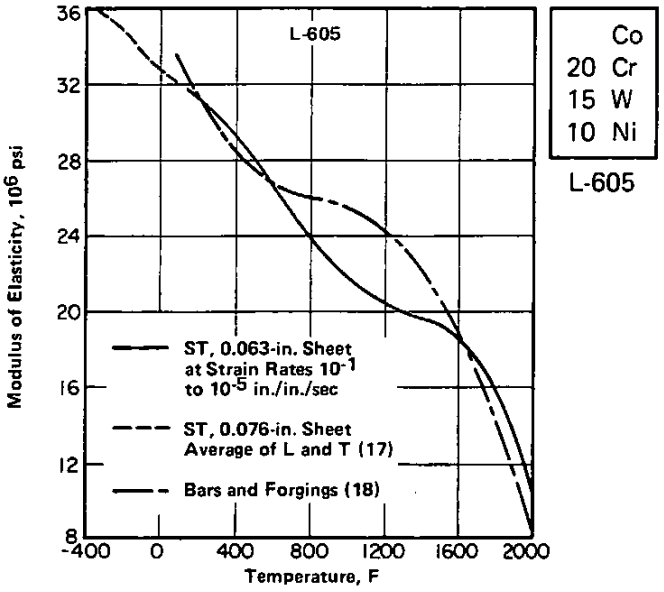

FIGURE 3.0621. MODULUS OF ELASTICITY IN TENSION (8,17,18)

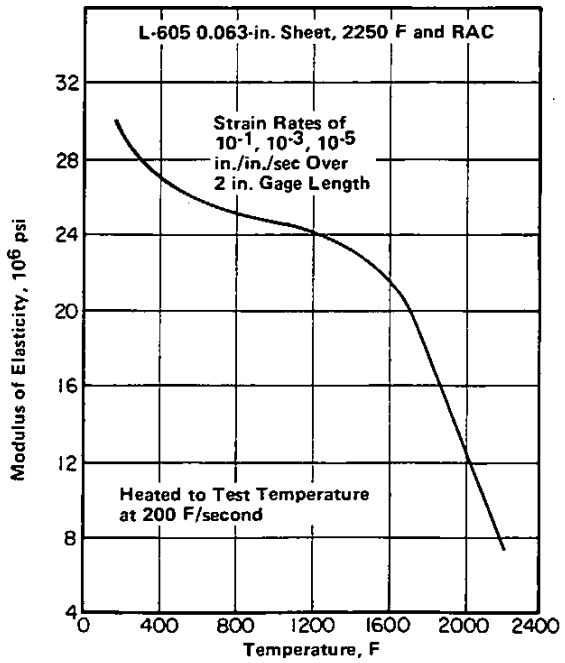

FIGURE 3.0622. MODULUS OF ELASTICITY OF SHEET IN COMPRESSION (30)

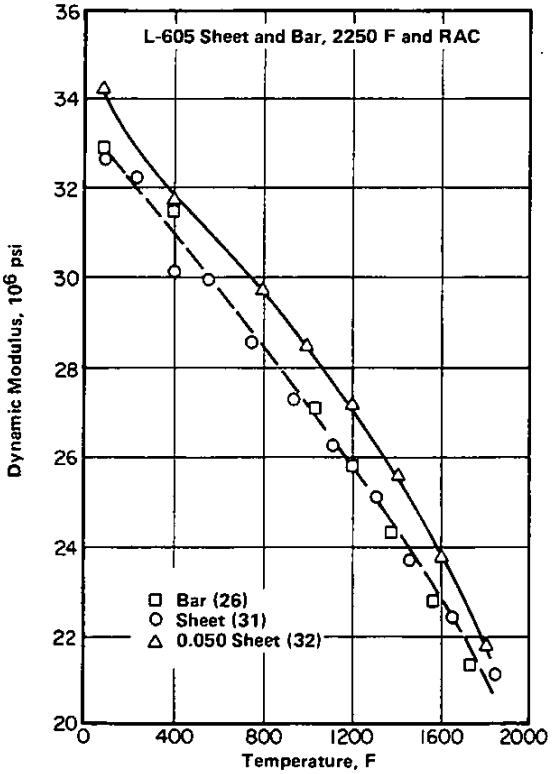

FIGURE 3.0623. DYNAMIC MODULUS AT ROOM AND ELEVATED TEMPERATURES (26,31,32)

Co
20 Cr
15 W
10 Ni
L-605

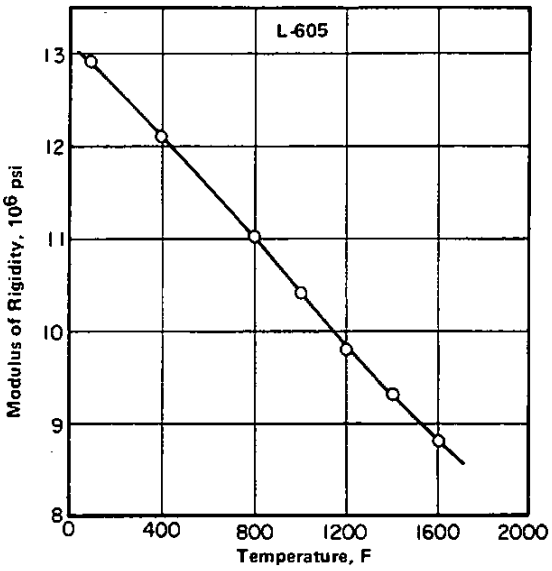

FIGURE 3.063. MODULUS OF RIGIDITY (62)

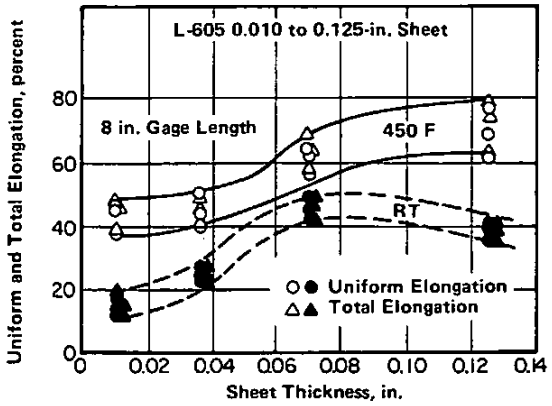

FIGURE 4.012. UNIFORM ELONGATION AND TOTAL ELONGATION FOR 8-INCH GAGE LENGTH OF SHEET DEFORMED IN TENSION TO SIMULATE FORMING OPERATION AT ROOM TEMPERATURE AND 450 F (37,57)

L-605		
Sheet Thickness, inch	Cold Reduction, percent	Cup Depth, mm
0.020-0.023	10	8.4
	15	6.8
	20	5.9
0.050-0.057	10	8.2
	15	6.7
	20	5.5

TABLE 4.013. ERICHSEN CUP TEST DATA FOR COLD-REDUCED L-605 (94)

L-605(a)				
Roll Sleeve Material	Roll Surface Temperature, F	Strip Lubricant	One-Pass Reduction, percent(b)	Roll Separating Force, lb
Waspaloy	70	(None)	29.0	106,000
	70	(None)	31.6	114,000
	70	GL-100(c)	41.0	70,000
	70	GL-100	44.4	62,000
	1500	(None)	30.8	104,000
	1500	(None)	31.6	104,000
IN-100	1500	(None)	30.8	80,000
	1500	(None)	32.5	78,000
	1500	(None)	34.2	80,000

(a) 1-inch-wide by 0.117-inch-thick strip.
(b) L-605 strip preheated to 1750 F. Roll speed 100 fpm. All test specimens fabricable with no edge or surface cracking.
(c) GL-100 is a phosphate glass.

TABLE 4.015. WARM ROLLING WITH HEATED ROLLS OR WITH LUBRICANT (78)

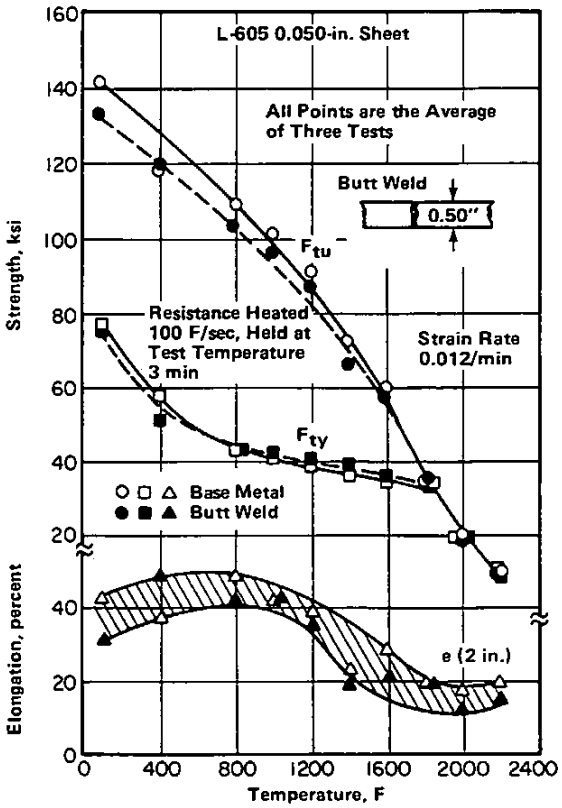

FIGURE 4.033. EFFECT OF TEST TEMPERATURE ON TENSILE PROPERTIES OF UNWELDED AND BUTT-WELDED SHEET (32,57)

Co
20 Cr
15 W
10 Ni
L-605

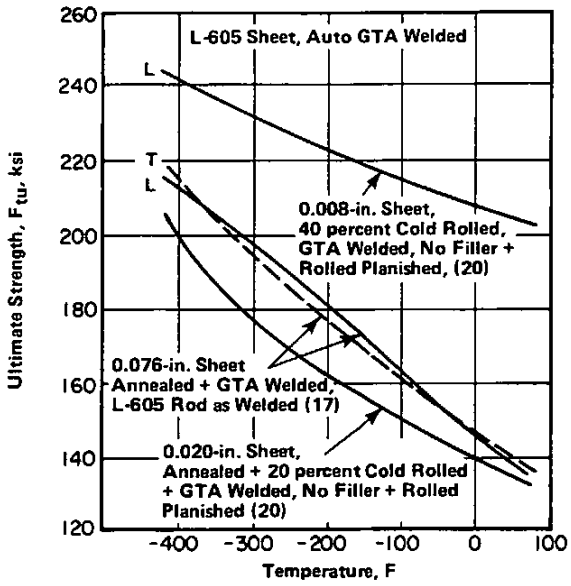

FIGURE 4.034. EFFECT OF LOW TEST TEMPERATURE ON TENSILE STRENGTH OF GTA WELDED SHEET (17,20)

L-605[a]				
Test Temperature, F	Braze Alloy	Ultimate Strength, ksi	Failure Location[b]	Joint Efficiency[c]
70	(None)	150	–	–
	J8400	109.5	B	73
	J8100	74.7	B	50
	CM52	78.9	B	53
	J8600	132.0	B	88
1800	(None)	25.7	–	–
	J8400	21.5	P	84
	J8400	19.3[d]	B	75
	J8100	22.0	P	86
	J8100	19.8[d]	B	75
	CM52	20.1	P	78
	J8600	0.6	B	2
2000	(None)	12.8	–	–
	J8400	12.9	P	101
	J8400	12.0[d]	P	94

(a) 0.010-inch sheet, solution heat treated.
(b) B = braze joint; P = parent metal.
(c) Joint efficiency = (F_{tu}, braze joint)/(F_{tu}, parent metal).
(d) After air exposure for 100 1-hour cycles to test temperature, 16-hour total exposure time at test temperature.

TABLE 4.035. TENSILE STRENGTH OF BRAZED T-JOINTS AT ROOM AND ELEVATED TEMPERATURES (95)